Integrated Optoelectronic Switching Technology for Fiber-Optic Communications Networks

A Study done for Astarte Fiber Networks, Inc.
and
The U.S. Army Space & Missile Defense Command

Regis Fan
R. Brian Hooker
December 23, 1998

Table of Contents

Integrated Optoelectronic Switching Technology for Fiber-Optic Communications Networks

Abstract

Optical switching can be performed by using optical amplifiers combined with a passive waveguiding network. Recently, most of the effort in optical amplifier switch modules have been focused on monolithic switches in which the entire device is fabricated on an InP substrate together with the semiconductor optical amplifiers (SOAs). In this paper, we investigate the use of SOAs with passive polymer waveguides to make hybrid switches of varying sizes. The optical amplifiers serve a dual purpose. The SOAs are used in order to gate the signal and amplify the signal in order to offset the losses associated with the passive waveguide elements as well as the losses from component misalignments in the switch module. Our analysis finds the largest switch module size that can be made with the architecture used. We also calculate the maximum number of switch modules which can be cascaded in order to retain a bit error rate (BER) under 10^{-9}.

1. Introduction

Optical switching has been a major area of interest since the advent of optical communication systems. There are several different types of optical switches including mechanical, directional coupler, Mach-Zehnder, and optical amplifier switches. Mechanical switches suffer from relatively slow switching speeds. It is difficult to obtain high extinction ratios with directional coupler and Mach-Zehnder switches which can lead to unwanted crosstalk. Recently, there has been much attention to optical amplifier switches since they have large extinction ratios and also have to ability to amplify the signal to offset the losses which are present.

There have been many researchers who have looked into making switches with optical amplifiers, as long ago as the early 1980's [1]-[2]. Since then, most optical switches using SOAs have focused on making a monolithic switch in the same material containing the SOA. This approach can help alleviate the misalignment between the passive waveguide routing part of the device and the amplifiers, however these devices often require complicated multistep epitaxial growth and complex processing [3]. There have been devices made at wavelengths of both 1.3 μm and 1.55 μm. Several different 2×2 monolithic SOA switches which have been made at AT&T Bell Labs [4], France Telecom [5], British Telecom [6], Ericsson Components [7], the Institute of Quantum Electronics in Zurich, Switzerland [8], NEC Corp.[9], and the Electronics and Telecommunications Institute in Taejon, Korea [10]. There have also been 4×4 switches made by Ericsson Components [11]-[12]. A hybrid technique for making a 4×4 optical switch using silica-based optical waveguides and SOAs [13] was described by NTT Opto-electronics Laboratories.

There have been many studies on lightwave systems using optical amplifiers, including switches. The propagation of amplified spontaneous emission (ASE) noise through lightwave systems has been studied by several researchers [14]-[18]. The effect of residual reflectivity on the SOA end facets has been analyzed [19]. The reflections between the waveguide and the SOAs were also investigated, and seen to be a large factor in a hybrid optical switch using silica-based waveguides [13]. In other studies, the crosstalk implications in optical networks have been analyzed and are shown to effect the signal to noise ratio of optical systems [20,21]. The impact of the input signal power on SOA switch systems have been investigated [22]. Effects of the input polarization state on SOA-based switches was also studied [23].

The structure for the optical switch under investigation is shown in Fig. 1 a) and b). It is shown for a 2×2 and a 4×4 switch. Larger switches can also be designed using the same type of architecture which is called a Matrix Vector Multiplier (MVM) switch [14][20]. In these switches there is only one SOA which is traversed for any branch of the switch. Thus, this single SOA is used for gating as well as for amplifying the signal to counter losses in the passive polymer waveguide network, as well as the losses from the misalignments and mode mismatch.

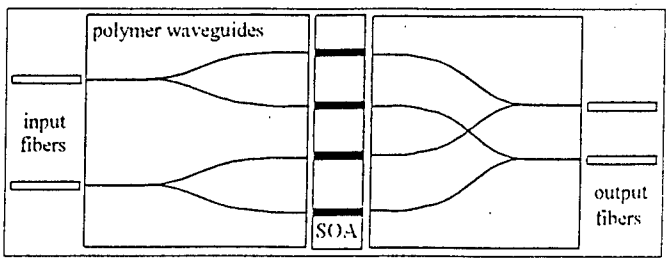

a) 2×2 switch module.

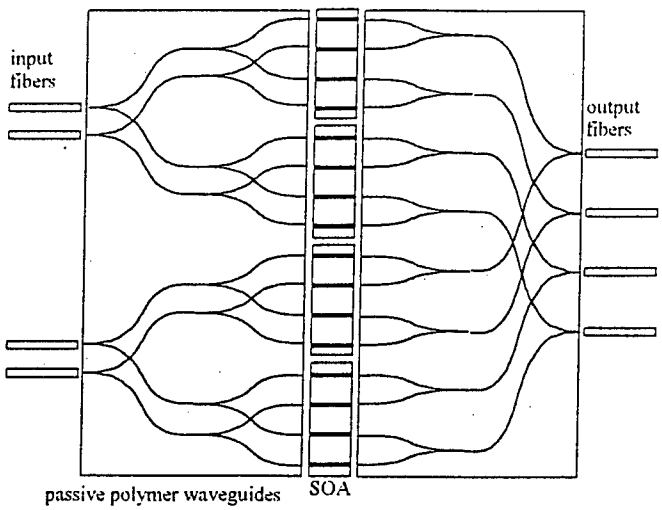

b) 4×4 SOA switch module.

Figure 1. Hybrid SOA switch module.

1.1. Overview of Program Objectives

Objective	Description	Priority
1	Polymer waveguide materials	High
2	Polymer waveguide designs	High
3	Module design and alignment techniques	High
4	Array size in view of device SNR	High
5	Acquisition of SOAs	High
6	Size granularity of integrated modules	High
7	Control of switching devices	Medium
8	Optical and electrical packaging	Medium
9	Yield/redundancy tradeoffs for SOAs	Low

Table 1. Project objective priorities

In the initial stages of the project, we prioritized the different objectives to determine the importance of each of objectives. Table 1 summarizes the objectives and their respective priorities. The first 6 objectives were found to be of the highest priority. Objectives 2, 3, 4 and 6 deal with the basic concepts imperative to the feasibility analysis of the hybrid switch and overall switching array size. Objective 1 allows us to determine the properties of the polymer available to make the polymer waveguide sections of the device, and Objective 5 deals with the acquisition of the SOAs which are necessary in order to make the hybrid switch. There are 2 medium priority objectives, of which the more important areas were analyzed. The low priority objective dealing with redundancy was not addressed.

In this report, we summarize the work involved with the design of an integrated optical switch using semiconductor optical amplifiers (SOAs) and passive polymer waveguides. In Objective 1, We start by describing the polymer materials that have been identified as candidates for use in the passive polymer waveguide section. Objective 2 describes the waveguide designs and design considerations dealing mainly with the losses in the waveguide section, including the use of tapers for mode transformation as well as other loss mechanisms. In Objective 3, we look at the module design and alignment techniques which includes a Monte Carlo analysis which shows the effect of the misalignment of the different components in the module. In Objective 4, we look into the maximum switch array size, taking into account the BER and gain saturation of the SOAs. We also find the maximum number of stages which can be cascaded, in order to find the switching array size that can be made using the smaller switch modules as building blocks. In Objective 5, we discuss the availability of SOAs which can be used in the hybrid optical switch. Objective 6 deals with the size granularity of the integrated module using results from Objective 4. In Objective 8, we look at some of the optical packaging issues with the hybrid switch.

2. Objective 1: Polymer waveguide materials

We have performed a paper study to find many of the common polymer materials currently used for photonic applications. The main types of polymer materials include acrylate based polymers [24]-[29], polyimides [30]-[33], siloxane polymers [34],[35], as well as several other various materials [36]-[43]. Acrylates have a low thermal stability compared to both the polyimides and the siloxane polymers. There are many different fabrication techniques. Currently, the major fabrication methods include RIE, wet-etching, embossing, and UV irradiation.

One of the problems with polymer materials has been the absorption loss of the materials. The C-H bonds have vibrational overtones which are most pronounced at wavelengths longer that 1 μm, with windows of transparency at 1.31 and 1.55 μm [26]. It is possible to substitute deuterium or fluorine for the hydrogen, in order to replace the C-H bonds by C-D or C-F bonds. This substitution leads to a reduction in the absorption loss in the near-IR region [44],[45]. These substitutions can be done in both acrylates, siloxanes and polyimides.

Polyguide is a material made by Dupont which is an acrylate polymer technology which can be used to make polymer waveguides. It has an effective T_g of about 150 °C, and comes in both a laminatable film and a liquid photopolymerized form. It has an optical loss of 0.2 dB/cm at 1330nm, and 0.6 dB/cm at 1550nm, comes as a laminatable film. The film is layered and is also photobleachable. The laminatable films are photosensitive, and can be layered to form a multilayer waveguide structure [24]. Both single and multimode waveguides are fabricatable.

PMMA (poly(methyl methacrylate) or Plexiglass™ or Lucite™) is another common polymer material currently used for photonic waveguide device fabrication. However, it has a glass transition temperature (T_g) of about 110°C, which is too low for many optoelectronics applications [46]. Although it does have good optical qualities which makes it a good material to use as a test vehicle. It can be used with a variety of fabrication techniques. It can be used with a dye in either a guest host, or side chained polymer system. PMMA/DR1, which is a side-chained material system has been developed by IBM which is a photobleachable material. PMMA can also be used without a dye and patterned by embossing at NTT [27], UV-exposure at the Institue of Applied Physics in Darmstadt, Germany [28], liquid jet delineation at Alabama A&M University [29]. It can also be used in conjunction with other materials to make waveguiding structures a the University of Dortmund [25].

Epigem Ldt. is a company based in England which also has a polymer material for use with polymer waveguide technology. The materials which they have use methacrylate groups with azo-dyes included within the polymer matrix [47]. The buffer material has an intrinsic loss of <0.1 dB/cm at 1300nm and 0.9 dB/cm at 1550nm. The guiding layers are photosensitive and can be photodefined to make the channels.

Other materials are siloxane based polymer materials. Like polyimides, polysiloxane materials have a high temperature stability. At NTT, waveguides have been made using a deuterated polysiloxane using RIE to form the channels [35]. Waveguides have also been made out of polysiloxane polymer at Kyocera also by RIE [34]. Waveguide losses in polysiloxane materials are about 0.15 dB/cm at a wavelength of 1.31 μm. There is also a material that looks like a polysiloxane, called ORMOCER™ which is an inorganic-organic polymer, with channels being defined by mold replication [37].

There are a number of other polymer materials which are used to make optical waveguides including perfluorocyclobutane (PFCB) which has losses less than 0.25 dB/cm at both 1.31μm and 1.55μm [39]. PFCB has losses that are much lower than benzocyclobutane (BCB). At Honeywell, waveguides using BCB as the cladding and a polyetherimide (ULTEM from GE) as the core have been made using RIE [48]. Akzo Nobel has a proprietary technology for fabrication of polymer integrated optical circuits using spin coating to build 3 layer structures [41].

The polyimide polymers have been used by several different groups including Hitatchi who used a fluorinated polyimide to make 2-dimensional mode size transformers [30]. The channels were defined by electron beam exposure. Amoco Ultradel 9020D (is a highly fluorinated pre-imidized polyimide) is another material that has been used by a couple different research groups [32],[33]. The waveguides were made by either wet-etch or RIE.

Another polyimide material is also made by Amoco called Ultradel 4212 which is a thermally cured polymer. This is one of the polymer materials which we have, and with which we have made waveguides. Amoco Ultradel 4212 can be doped with DCM dye (4-(dicyanomethylene)-2-methyl-6-(p-dimethyl aminostyryl)-4H-pyran) for use in a guest/host system. A guest/host system is one in which the dye is not chemically attached to the polymer backbone (such as in a side-chained or copolymerized polymer material system), but is simply mixed together with the polymer. We have made 3 layer polymer waveguides using 4212/DCM in our clean room at the University of Colorado. To prepare 4212/DCM solution, DCM is first dissolved in NMP (1-methyl-2-pyrrolinone) solvent. After a few hours, when the dye is totally dissolved in the NMP, the solution is filtered through a 0.2μm filter. The Amoco Ultradel 4212 polyimide is then added to the filtrated solution. The weight ratio between the 4212 and the NMP will define the obtainable thicknesses of the films, and the weight ratio between 4212 and DCM will define doping concentrations. Commercial Amoco Ultradel 4212 is a 17.8% solution of 4212 in diglyme. 4212 is a thermally cured material and has a glass transition temperature (T_g) of 295°C. The absorption coefficient of Ultradel 4212 is about 0.8 dB/cm at 1330nm and 0.13 dB/cm at 1550nm. Amoco also makes another polyimide polymer named Ultradel 9020D. This is a similar material to 4212, but is a UV curable polymer.

3. Objective 2: Waveguide designs

In this section, we look at the waveguide design considerations. We begin by analyzing the individual loss mechanisms in the polymer waveguide section. There are several different loss mechanisms including mode mismatch and waveguide taper loss, splitter/combiner loss, channel crossings, channel bends, component misalignments, and other channel losses such as imperfections and sidewall scattering. We start by analyzing these individual losses, using Beamprop (Rsoft Inc.), after which we look at the waveguide losses for a 2x2 and 4x4 switch module, excluding the mode mismatch and misalignment losses. The mode mismatch and misalignment losses are analyzed in Objective 3, using a Monte Carlo approach.

3.1. Tapered polymer waveguides and mode mismatch

Each component in the hybrid integrated optoelectronic switch has a structure that is optimized for its operation, and the mode sizes and shapes of different components often have mismatches which make coupling between them challenging. Therefore, there needs to be an efficient way to transform modes from one shape and size to another. One way of performing this mode transformation is through the use of a tapered waveguide.

The tapered waveguides that we are developing are made of polymer materials. In this section we start by introducing our 3-dimensional polymer tapered waveguide structure. We then describe the polymer waveguide material system which we use, and the fabrication technique for making waveguides.

3.1.1. Tapered structure

The tapered waveguide structure which is used for mode transformation is shown in Figure 2. With the structure in Figure 2, a taper can be made to transform the mode in the vertical as well as the lateral direction. The structure consists of two waveguiding layers. One of the layers contains the portion of the waveguide that forms the input section. This layer may also contain a lateral taper if the input waveguiding structure has a different width than the output structure. The second layer has its guiding region directly above the lower guiding layer, and contains a lateral taper that up-tapers from zero width. So the mode traveling down the waveguide sees a smooth transition. There is a straight section at the input and output of the waveguide.

This taper cannot be strictly adiabatic since there is a discontinuity in the slope of the structure in the vertical direction. However, since the channel width up-tapers from zero, the change in the shape of

the mode is gradual. This gradual change can keep the radiation loss to a minimum. Lateral tapers are easily made, since the channels are defined by photolithography and the polymer layers are planar. These polymer channels can be made quasi adiabatic, as long as the mask containing the channel defining structure has a smooth taper structure with a small taper slope.

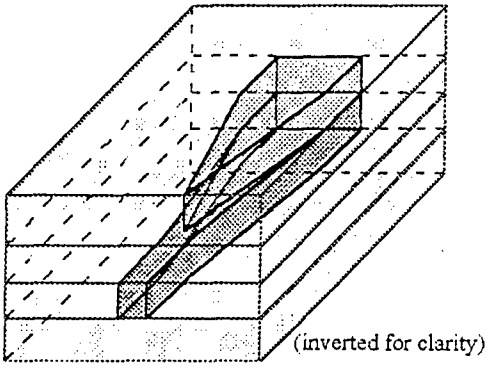

Figure 2. 3D tapered waveguide structure.

3.1.2. Polymer waveguide fabrication

The polymer which we currently use is Amoco Ultradel 4212 polyimide combined with DCM dye. The polymer and chromophore are used in a guest/host system. A guest/host system is one in which the chromophore is not chemically attached to the polymer backbone. The guest/host system is different from a side chained or a copolymer system, in which the dye is attached to the polymer. For a guest/host system the dye is dissolved in a solvent and mixed with the polymer. A certain amount of chromophore can be added to the polymer before the optical quality degrades. For DCM/4212, this maximum concentration is a little over 10% by weight, which creates a maximum index of refraction change of about 0.015 when the polymer system is bleached to saturation.

The polymer layers are spun onto a silicon substrate, where the layer thickness is determined by the spin speed. Once a doped layer is made, a channel can be defined by masking and exposing it to UV light. The areas that are exposed to the light decrease in refractive index. The index change can be found using a model for calculating the index change for a given dye doping and light source intensity [49].

In order to make the 3-dimensional structure of Figure 2, the layer which up-tapers from zero width must be spun and exposed first. This is so that when the layer above it is bleached, the mask will also shade the unexposed area of the first guiding layer. If the layers are bleached to saturation, more exposure to the cladding area does not change the index further.

The structures that we have thus far successfully fabricated are shown in Figure 3. These waveguides are made with undoped 4212 polyimide as the buffers with a DCM/4212 guiding layer. The substrate that we use is a 2 inch silicon wafer with a 1.5 μm SiO_2 oxide layer. The bottom buffer, undoped 4212 polyimide, is spun onto the substrate and cured. Next, the guiding layer, DCM/4212, is spun onto the buffer layer and baked. Then the channels are defined using a mask and bleaching with UV light. The top buffer (undoped 4212) is spun cast and baked. Finally, the channel end faces are prepared by dicing with a diamond grit blade.

The 4212 polyimide guiding layer contains 10% DCM dye by weight. The index of refraction of undoped 4212 is 1.57425. The unbleached 10% DCM in 4212 has an index of 1.603407, and has an index of 1.589 when bleached to saturation. So the maximum lateral index step (Δn) is about 0.015 for the 10% DCM in 4212. Since the bleaching is a function of exposure, we can choose the lateral index step by bleaching for the appropriate time [49]. The index step between unbleached 10% DCM/4212 and 4212 is about 0.03.

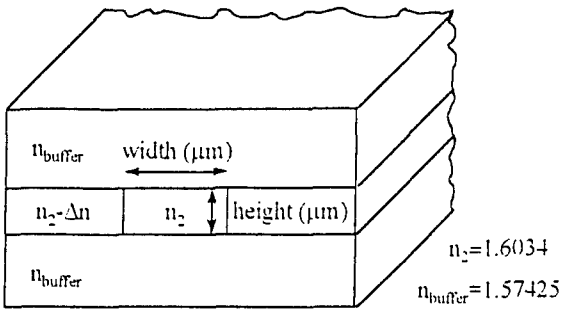

Figure 3. Waveguide structures fabricated.

We have been able to make good quality three layer structures. However, there have been certain processing difficulties associated with making a four layer, two guiding layer, waveguide structure that is shown in Figure 2. The dye sublimes at a temperature lower than the thermal curing temperature for 4212. If the layer is baked at a lower temperature than the curing temperature, the layer is not as strong. We have observed cracking in a non-cured layer of DCM/4212 when another layer is spun on top of it. We have also observed that solvent can attack a partially cured DCM/4212 layer that has been bleached. The index values of our polymer material system are typical of those of other polymer materials, so the designs that follow are adaptable to other material systems.

3.1.3. Tapered waveguides for SOA and fiber coupling

In this section, we use a model to analyze an example of how a tapered waveguide can be used to perform a specific mode transformation. We treat the problem of coupling light from an SOA to a fiber. In this example, a waveguide is used to perform the mode conversion from the small elliptical SOA distribution to that of the larger circular fiber profile. A technique such as self-aligned flip chip soldering can be used to passively align the waveguide to the SOA [50].

Tapered waveguides can be used to transform from the elliptical mode to the circular fiber mode. If the taper is adiabatic, the energy remains in the mode that is excited and there is minimal radiation loss. The waveguide need not remain single mode because, for example, if the fundamental mode is excited, then the energy remains in that mode only. In order to have the best coupling efficiency, the mode shapes should be well matched.

3.1.3.1. Optimal index profile for SOA to fiber coupling

In a previous analysis, we have shown some of the design considerations when designing polymer waveguides for coupling between different structures [51]. We found that there needs to be a high index step at the input in order to couple well between the polymer waveguide and a SOA. The large index step is desirable so that we can obtain a small, tightly confined mode which has as large an overlap with the SOA mode as possible. We also found that a low index step at the output is desirable to well match the index step in a fiber.

Figures 4 and 5 show the input and output index profile and structure of the 4 layer waveguide, respectively, which are used for the simulations in the following section. As can be seen, the index values are the same as those shown in Figure 3, and correspond to 10% DCM in 4212. Figure 5 shows the output structure from which we can see that the core extends into both middle (guiding) layers, and has an index of n=1.592407. The top and bottom cladding and the side cladding indices are the same as the input side. In order to have these input and output structures, it is evident that a grading of the core index is necessary.

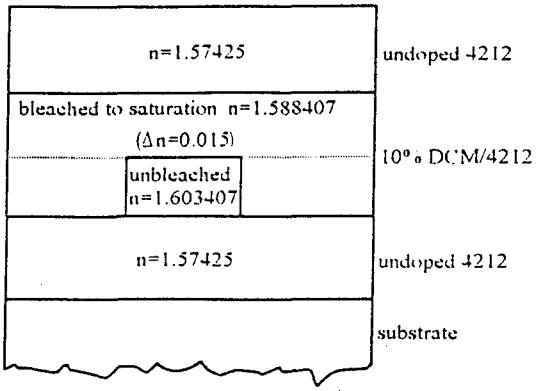

Figure 4. Input structure and index profile.

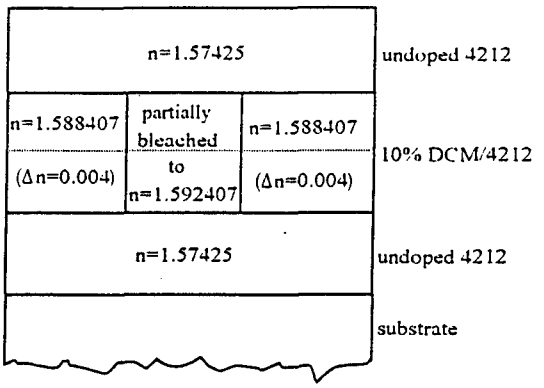

Figure 5. Output structure and index profile.

3.1.3.2. Design and analysis of 3D structure

The design of an optimal tapered waveguide structure depends on the waveguide structures we are coupling between. In order to model the waveguide coupling, the modes of the waveguide were found using BeamPROP by RSoft, Inc which uses a finite difference solution to the wave equation with transparent boundary conditions. The coupling efficiencies were found by performing an overlap integral between the waveguide distributions and the input (SOA) or output (fiber) mode.

We begin by modeling the coupling between a SOA and the polymer waveguide, followed by the coupling from the polymer waveguide to an optical fiber. We use the index profiles from the previous section, and vary the physical dimensions to obtain the highest coupling efficiencies for both the input and output. Next, the propagation of light through the 3-dimensional taper is shown, and finally the issue of adiabatic tapers and taper length is addressed.

3.1.3.2.1. SOA to waveguide coupling

To calculate the coupling efficiency from a SOA to a waveguide, the SOA distribution must be known. The near field SOA distribution that is emitted from the SOA was found by using the FWHM intensity angles of the SOA in the far field. The SOA structure was approximated by choosing typical values for the index of refraction and dimensions of a SOA that operates at 1.3 μm (made of InGaAsP). The effective index method was used to calculate the mode profile of the SOA. Then the parameters of the SOA structure were varied until the far field angles matched the given angles of our SOA. The vertical FWHM angle was 35° and the lateral FWHM angle was 17°.

For the waveguide input, we found the mode of the waveguide using BeamPROP. An overlap integral was calculated between the waveguide mode and the approximated SOA mode. It was assumed

that the SOA and waveguide were in contact, and the coupling efficiencies were calculated for different vertical and lateral misalignments.

The index of refraction values from Figure 4 were used, which correspond to the highest index steps available with our material system. The core dimensions of the waveguide were varied, and the coupling efficiencies calculated for the different channel sizes. In Figure 6 the peak efficiency is graphed for the different waveguide dimensions. Each curve corresponds to a different channel height and the peak efficiency is shown for varying channel widths.

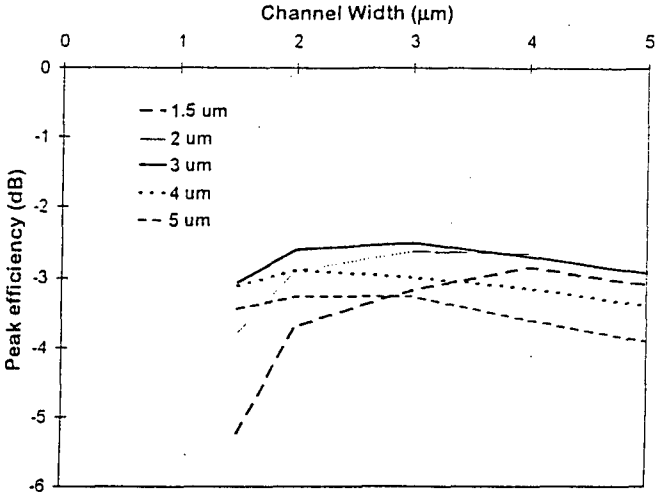

Figure 6. Peak coupling efficiency of SOA into 3D tapered waveguide structure.

In Figure 7 the misalignments which cause a 3dB excess loss from the peak efficiency are plotted for the channel with the 3μm height. Both the lateral and vertical 3dB loss values are plotted. Since the input has an asymmetric index composition in the vertical direction, the mode is also asymmetric. The mode is more tightly confined by the lower cladding, where the index step is greater ($\Delta n \sim 0.029$) and is less tightly confined above the guiding region where the index step is lower ($\Delta n = 0.015$). Thus the average of the two 3dB misalignments is plotted. The input structure which provides the highest coupling efficiency is the 3×3 μm channel which has a peak coupling efficiency of -2.5 dB or about 56%. It has an average vertical 3dB misalignment value of 1.29 μm, and a lateral 3dB misalignment of 1.56 μm.

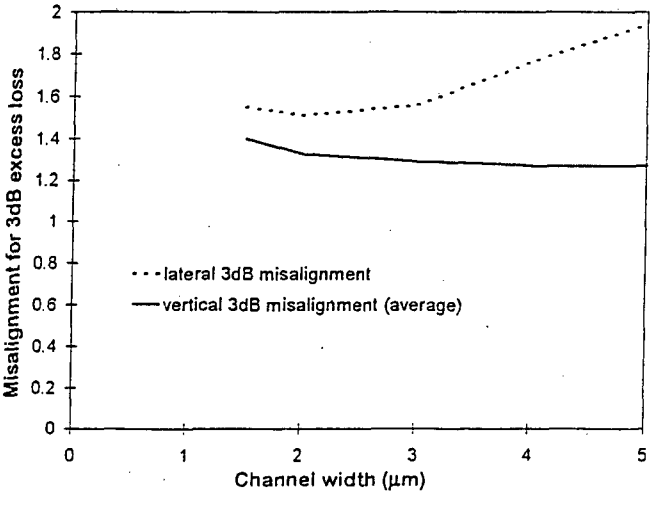

Figure 7. Misalignment which causes a 3dB excess loss from the peak coupling efficiency with a 3 μm channel height.

3.1.3.2.2. Waveguide to fiber coupling

In order to design the output of the 3D tapered waveguide structure, we performed a similar analysis to that of the previous section. The fiber mode was found using the standard Gaussian approximation of the mode [52]. We used the structure and index values shown in Figure 5. From a previous analysis, it was found that the input coupling is more challenging to maximize than the output to fiber coupling, and that high index steps are needed. Thus we used top and bottom buffers that would give the highest index values possible. This then constrained the output structure to a fairly high index step in the vertical directions. Ideally, we would like to have a square output structure with low index step values of Δn=0.004, similar to that of a standard single mode optical fiber [51].

In order to maximize the output coupling, we used a longitudinal index taper that reduced the core index and produced the index profile in Figure 5. The core index was reduced in order to lower the index steps in both the vertical and lateral directions. The core index was reduced to produce a lateral index step of 0.004, making the vertical index step a little under 0.018.

Table 2 shows the coupling efficiency, as well as the offsets which cause a 3dB drop in the coupling efficiency, at the waveguide output to a fiber. The results for several different geometries and index values are shown. The first 2 entries are for a 4x4 and a 5x5 channel where there is no longitudinal index taper. In these two cases, the index step was kept at Δn=0.015 throughout the length of the tapered structure instead of grading the index to Δn=0.004 at the output. It can be seen that the peak efficiency is lower for these two entries than for the case of using the longitudinal index taper. The longitudinal index grading increases the coupling from 66% to 81% in the case of the 4×4 channel. The coupling increases from 73% to 86% in the case of the 5×5 channel. Thus we see that the tapering of the index increases the coupling from the waveguide to the fiber. The highest peak efficiency is about 91% and occurs for the 6×6 μm channel with the lower index step of Δn=0.004 at the output.

Dimensions in μm (width x height)	longitudinal index grading	Peak efficiency	lateral 3dB misalignment (μm)	vertical 3dB misalignment (μm)
4x4	no	65.78	3.14	2.9
5x5	no	73.12	3.2	2.98
4x4	yes	81.48	3.64	3.08
5x5	yes	85.83	3.72	3.06
5x6	yes	90.02	3.71	3.15
6x6	yes	91.15	3.79	3.17
6x7	yes	91.09	3.66	3.14
7x7	yes	90.76	3.77	3.12

Table 2. Peak coupling efficiency and 3dB misalignments for different output geometries.

3.1.3.2.3. Light propagating through the 3D optimized tapered structure

As seen in the previous 2 sections, the optimized input with the index values as shown in Figure 4 has dimensions of 3×3 μm. The output structure with the index profile as in Figure 5 has dimensions of 6×6 μm. In this section we examine the behavior of the light distribution as it propagates through a long tapered structure, and next we show the effect of reducing the taper length on the taper performance.

Figure 8 shows the cross sections of the light distribution as it propagates through a tapered structure illustrated in Figure 2 with the optimized input and output dimensions. It also shows a cross section of the waveguide structure at the corresponding location in the tapered waveguide. Figure 9 shows the top view of the waveguide structure that the light is propagating though. It can be seen that there is a 200 μm input section which is straight and a 600 μm section at the output which is also straight. The tapering occurs over 800 μm and starts after the 200 μm straight input section. The grading of the

index from $\Delta n=0.015$ to $\Delta n=0.004$ is linear and occurs over the same 800 μm section as the lateral dimensional tapering.

As can be seen from looking at the distribution at both the 0 and 200 μm distribution cross sections, the modes are the same and are asymmetrical about the channel. The mode is more tightly confined on the bottom, where the index step is higher. The mode begins to expand as it reaches the up-tapered section, and begins to grow into the second guiding layer as the layer up tapers from zero width. The mode transformation is complete once it has reached the end of the taper. The output mode is then symmetric in the vertical direction. We can also see from the contour plots of the mode that the output mode is more tightly confined in the vertical direction, and less in the lateral where the index step $\Delta n=0.004$ at the output.

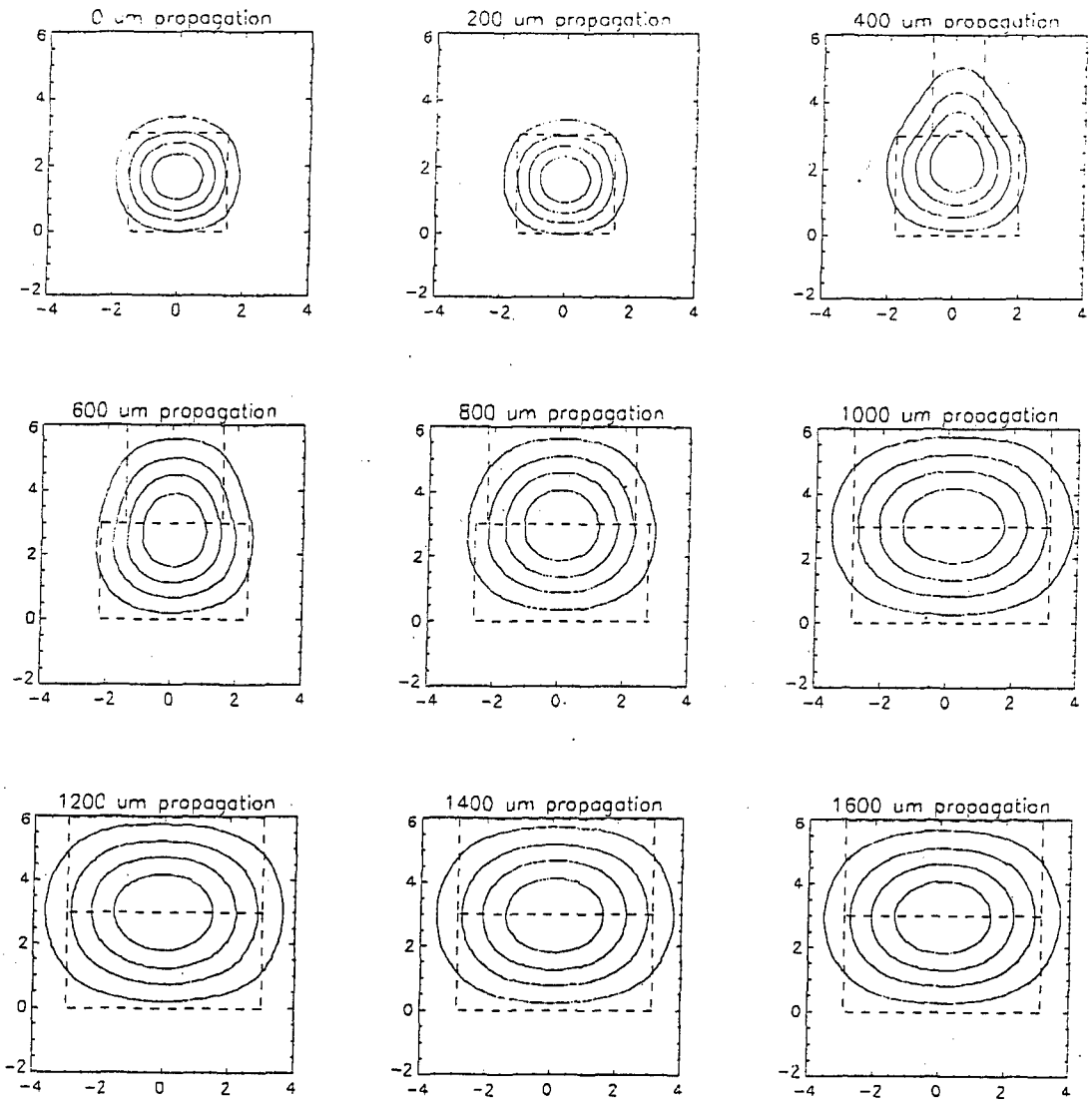

Figure 8. Mode of the tapered structure as it is being transformed from the input to the output of the waveguide (dimensions in μm)

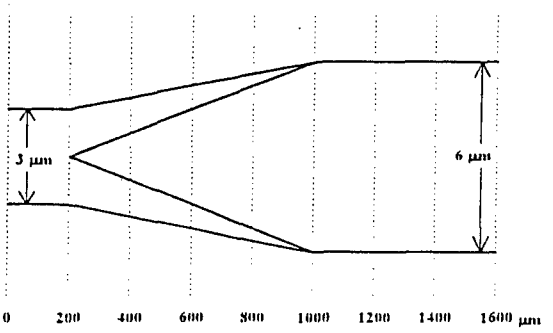

Figure 9. Top view of tapered waveguide structure showing where the cross sectional distributions and waveguide structures are sampled.

In Figure 10 we can see the total power through the tapered waveguide structure. The power is constant through the first 200 μm straight section, and then decreases most noticeably though the next 800 μm where both the lateral tapering and the index grading occurs. The guided power then stabilizes again for the last 600 μm straight section. There is under 1.5% loss as we propagate through the taper structure.

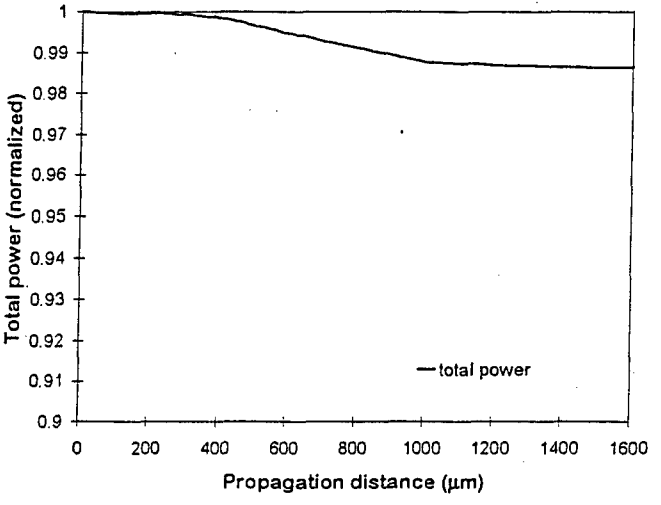

Figure 10. Total power (normalized) through taper.

Figure 11 shows the overlap integrals between the propagating distribution and both the fiber mode and the SOA mode. We can see that the SOA mode overlap at the input is 56%, as shown in Figure 6 for the 3×3 channel. As we would expect, the overlap with the SOA distribution decreases as the mode propagates through the taper since the mode is being transformed into the larger mode which is optimized to match the fiber mode. In Figure 11, we can also see the overlap of the fiber mode with the mode propagating through the taper structure, and this curve has the opposite trend from that of the SOA mode. We can observe that the overlap increases to its maximum value of 91%, as shown in Table 2 for the 6×6 waveguide output structure.

The overall coupling efficiency from the SOA to the fiber is a multiplication of the input coupling with the SOA, the output coupling with the fiber and total power at the output of the waveguide. The total coupling efficiency from SOA to fiber is therefore slightly higher than 50% or about -3dB.

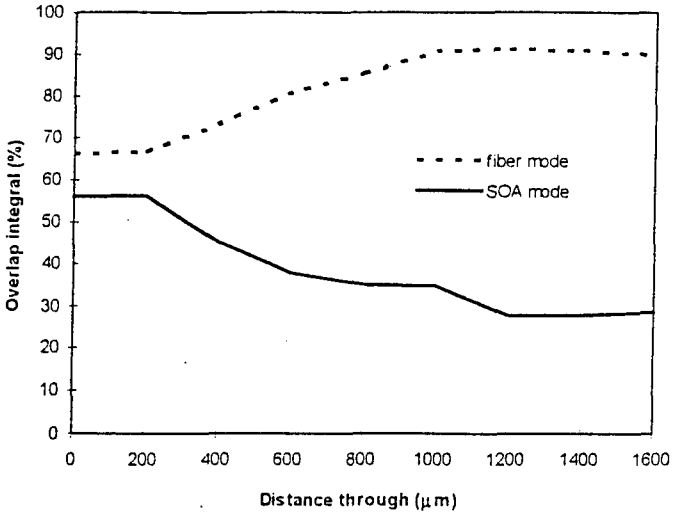

Figure 11. Overlap between propagating mode and fiber and SOA mode.

3.1.3.2.3. Adiabatic propagation and taper length

An adiabatic taper is a taper in which all of the energy remains in the initially excited mode, and hence the taper is lossless. It is possible to design a taper in a dielectric material which is lossless and this has been shown in several studies [53]-[57]. However, these completely adiabatic structures require precise control over taper shape and index profile. Using practical waveguide fabrication techniques, these structures would be impossible to make. If a photo-lithographic waveguide fabrication technique is used, the waveguide channel can be defined only as well as the mask can be made. Using standard mask making technology, there is the problem of discrete step sizes on the masks. There is also a problem of precise control of the refractive index for a graded index structure.

Since a lossless, strictly adiabatic taper cannot be fabricated, we must then design the taper to be low in loss. There are several ways to analyze a tapered waveguide in order to see the amount of loss that occurs. Several different techniques have been used to analyze taper structures, including intrinsic mode calculations [58]-[59], the step transition method [60]-[62], coupled mode calculations [63]-[65], and beam propagation techniques [66]-[67]. A general consensus that comes from these analyses on tapered waveguides is that if a taper is made long enough, and has a gradual enough taper slope, the taper can have low loss. And an infinite length taper would be strictly adiabatic.

If the loss is plotted versus the taper length or taper slope, a region can be found after which the taper loss is acceptable for the given application. It has been observed that taper lengths which are on the order of hundreds of microns can achieve low loss [60]. The taper shape then becomes less important, especially given the discrete step nature of masks. As seen the previous section, we have chosen a linear taper structure, which can be a suitable taper shape [62],[66].

We have analyzed the effect that the taper length has on our two guiding layer tapered structure. The taper length does have an effect on how the taper structure is able to transform the mode. Figure 12 shows the total power through the structure for taper lengths of 0, 100, 200, 400 μm, as well as for the 800 μm taper which we analyzed in the previous section. Figure 13 shows the overlap between the propagating mode and the fiber mode.

As we can see in Figure 12, the 400 and 800 μm tapers have about the same total normalized power at the waveguide output of about 98.5%. The 200 μm taper has a total output power of a little under 98%, the 100 μm channel has an output power of about 95%, and the total output power is down to about 85% for the 0 μm taper length.

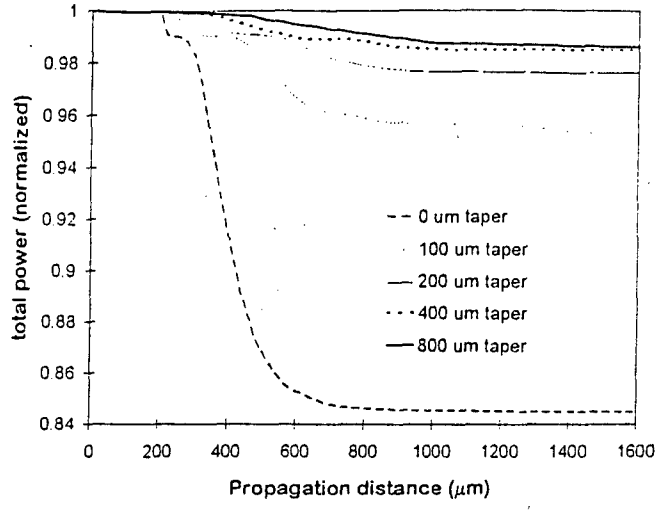

Figure 12. Total power propagating through channel for different taper lengths.

It is also interesting to observe that the coupling from the output of the waveguide to the fiber is not the same for all of the taper lengths, even though the output structure is identical. From Figure 13, we can see that the output coupling is the same for the 400 and 800 μm channels, but decreases as the taper lengths decrease.

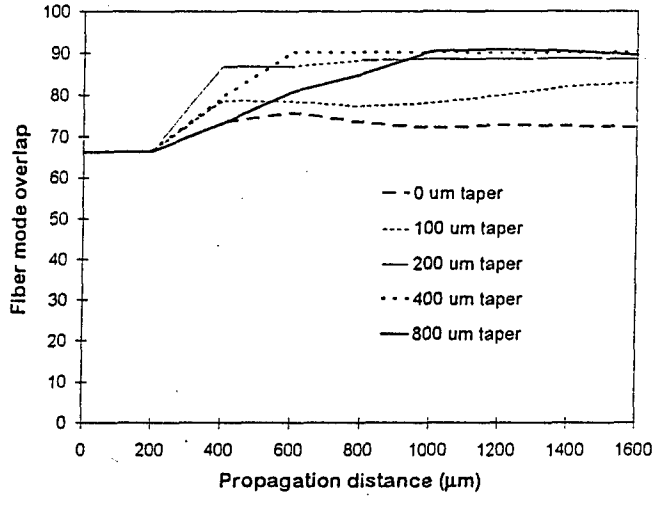

Figure 13. Overlap between propagating mode and fiber for different taper lengths.

If a waveguide structure propagates only a single mode, we would expect the coupling to be the same from the waveguide to a fiber, since the channel could only carry one mode, and that one mode would be the same, independent of how it was exited (once the radiated light had all been radiated out of the transparent boundary). We have determined using the effective index method that the output structure of the tapered waveguide is no longer single mode, as it was at the input. This can have an effect on the coupling characteristics.

The longer tapers have the same coupling efficiencies to the fiber, and the same total output powers. They show adiabatic behavior, although they do have about 1.5% loss into the radiation modes (and therefore are not strictly adiabatic). These channels are propagating only the fundamental mode, which is the mode excited at the input end where the channel is single mode.

By observing the total power plot for the 0 μm taper length, we can see that it has a constant power level after propagating about 800 μm through the waveguide. This indicates that the radiated light has been removed from the computation window. We performed an overlap integral between the

distribution obtained from the 800 μm taper case to that of the 0 μm taper, giving us an overlap between the two output distributions of about 85%. Thus only 85% of the energy in the 0 μm taper case is being guided by the fundamental mode at the output of the channel. This explains why the coupling varies from waveguide to fiber with the same waveguide structure. The output coupling is only 72% from the waveguide to the fiber in the 0 μm taper case, compared to 91% for the longer tapers. This implies that there is energy that has coupled not only into the radiation modes, but also into the higher order modes in the waveguide.

From this analysis, a 400 μm taper is about the minimum length in order to have a low loss taper with good adiabatic behavior using this 3D taper structure. If the waveguide dimensions and/or index of refraction values were changed, this length would not necessarily be the same, since it is dependent on the waveguide structure.

3.1.4. Summary of tapered waveguide for mode transformation

We have designed a tapered polymer waveguide which can perform a mode transformation for improved coupling between waveguiding structures with different mode shapes and sizes. The structure we are developing has a 4 layer design and uses 2 guiding layers and only lateral tapers. It can, however, modify the mode in both the lateral and vertical directions. There is one layer that contains a tapered channel that up-tapers from zero width, and is positioned directly above the other guiding channel.

We have developed a methodology for designing tapered waveguides. A specific example of coupling a SOA to a fiber was analyzed. The input and output structures were optimized using the index values for our material system (DCM/4212), which are also typical of other optical polymer materials. The waveguide input (SOA side) has dimensions of 3×3 μm and the output (fiber side) has larger dimensions of 6×6 μm. A longitudinal grading of the index was used to obtain a lower index step at the output of the tapered waveguide for better waveguide to fiber coupling.

The 3-dimensional taper structure uses a tapered structure with linear lateral tapers and a linear index grading. We found that there is near adiabatic propagation if the structure is built sufficiently long, 400 μm for our example of SOA to fiber coupling.

We believe this same tapered polymer waveguide technology can be used to couple light between arbitrary optoelectronic integrated circuit components (e.g. switches, amplifiers, fibers) with different mode sizes.

3.2. Splitter loss

An ideal splitter/combiner has 3dB of loss. In a splitter, half of the light goes in each arm of the splitter. In a real device, there will be some finite loss. In order to get an idea of the magnitude of this loss, BeamProp was used to model a single S-bend and then an S-bend splitter. The splitter is simply an S-bend mirrored with respect to the initial straight channel. In order to find the splitter loss, the single S-bend loss was compared with the total splitter loss. If the splitter is loss-less, half of the power would go into each arm, so that the total power at the output of the splitter would be the same as the output power in the single S-bend, since the bends are identical and have the same loss. Thus, the loss due to the splitter was found by taking the difference between the output powers in the single S-bend and the S-bend splitter (mirrored S-bend). The analysis was performed for the optimized 3x3 μm channel for an S-bend with a 125 μm translation, which corresponds to a splitter with an ending channel separation of 250 μm. In Figure 14 below, we can see the losses of S-bend and splitter for several different S-bend lengths.

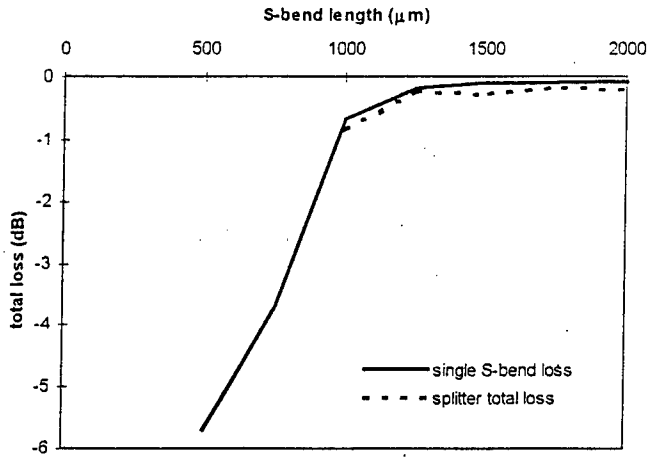

Figure 14. Losses due to a 125 μm S-bend and S-bend splitter.

The loss due to the splitter is the difference between the single S-bend loss and the total loss in the splitter. The splitter loss is shown in Figure 15. As can be seen, the average splitter loss has an value of about -0.1 dB, depending on the length of the splitter.

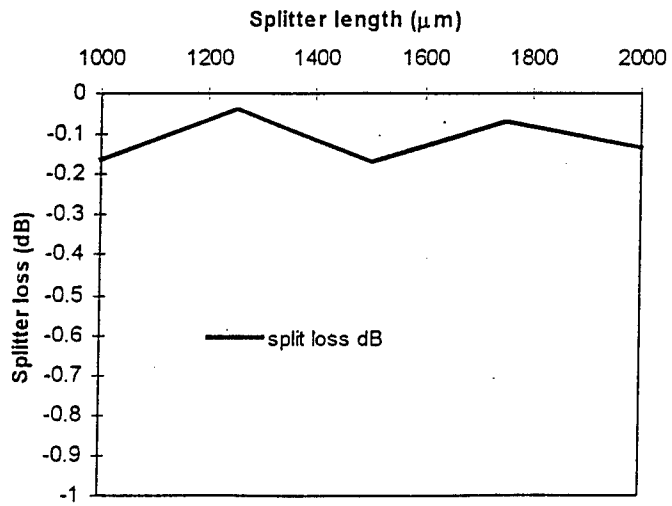

Figure 15. Difference between total S-bend splitter loss and single S-bend loss (splitter loss).

3.3. Channel crossing

This section shows the losses which occur when two channels cross at different angles. We analyze channel crossings for the optimized input 3x3 μm structure. As can be seen from the Figure 16 the loss is under 0.1 dB if the bend angle is over an angle of about 30°.

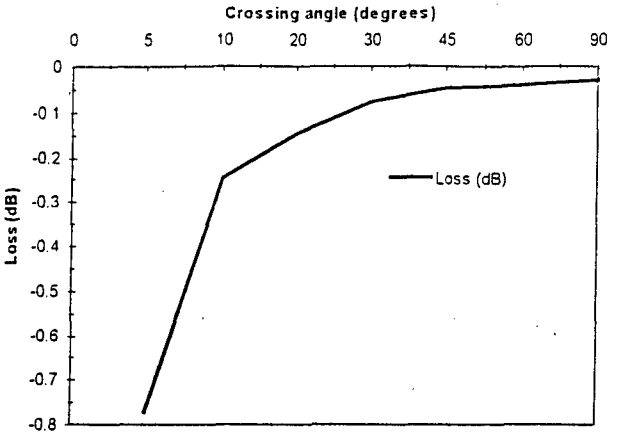

Figure 16. Loss for channel crossings.

3.4. Channel bends

We have already seen the losses due to an S-bend in Section 3.2. In this section we analyze the losses due to radial bends in the channel using a different technique. Beamprop can handle radial bends by transforming the entire problem space to effectively follow a circular arc. This is done by transforming the refractive index profile by multiplying it by $(1+x/R)$. This technique offers a simpler and more effective way to analyze bends, compared to a direct calculation using a constant propagation direction. For example, a radial bend of a channel over more than 90° cannot be done by propagating in one direction. In addition, the propagation step size must be decreased as the angle of the channel increases with respect to the propagation direction, thus increasing the computation time.

Figure 17 shows the loss as light propagates down channels with different radii of curvature. As can be seen, the loss increases for shorter radii. The loss in dB/cm was calculated from these curves and the values are shown in Table 3.

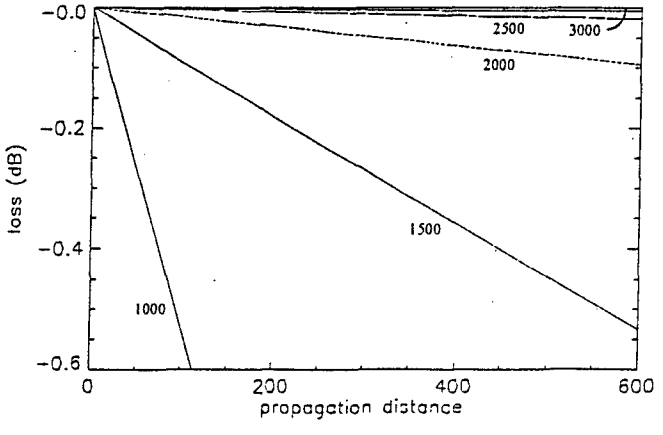

Figure 17. Loss vs propagation distance for different channel radii of curvature.

radius of curvature	loss (dB/cm)
1000	-5.26316
1500	-0.92308
2000	-0.15625
2500	-0.03175
3000	-0.00794

Table 3. Loss for different radii of curvature.

3.4.1. S-bends losses

In this section, we analyze waveguide S-bends, using the results for the loss for different bend radii, in order to determine the radius of curvature which should be used for best overall S-bend performance. An S-bend structure has the properties which are shown in Figure 18. We can derive a relationship between the length of the S-bend, the distance that the channel is translated in the x-direction and the radius of curvature of the S-bend.

$$R = \frac{\sqrt{L^2 + d^2}}{4\cos(\tan^{-1}(L/d))} \tag{3.1}$$

$$\theta = \tan^{-1}(L/d) \tag{3.2}$$

$$\phi = 90 - \theta \tag{3.3}$$

where L is the length of the S-bend, R is the radius of curvature and d is the translation distance. The length allows us to calculate the loss due to the channel bending using the loss values from Table 3, which shows the bend loss in dB/cm. The length will also come to play when we calculate the total loss which includes the waveguide channel loss (also in dB/cm) due to material absorption, sidewall scattering and other imperfections.

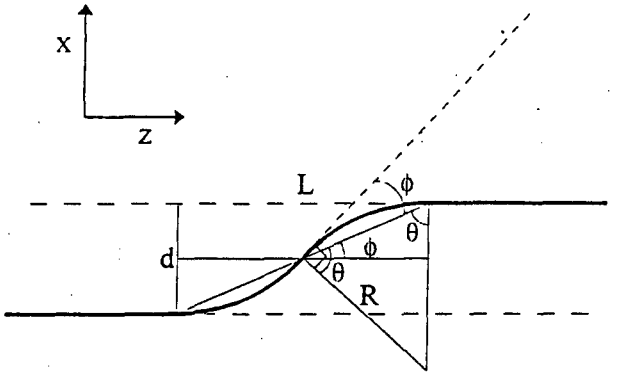

Figure 18. Properties of a waveguide S-bend.

Figure 19 shows the length of the S-bend as well as the S-bend loss as a function of the bend radius. As can be seen, the loss decreases as the radius of curvature increases. The length of the S-bend increases as the radius of curvature increases. We can also see that the loss increases as the channel translation increases. For all of the channel translations, the loss begins to plateau after a curvature of about 2000 μm. Therefore, we use S-bends with a 2000 μm radius of curvature in our waveguide designs.

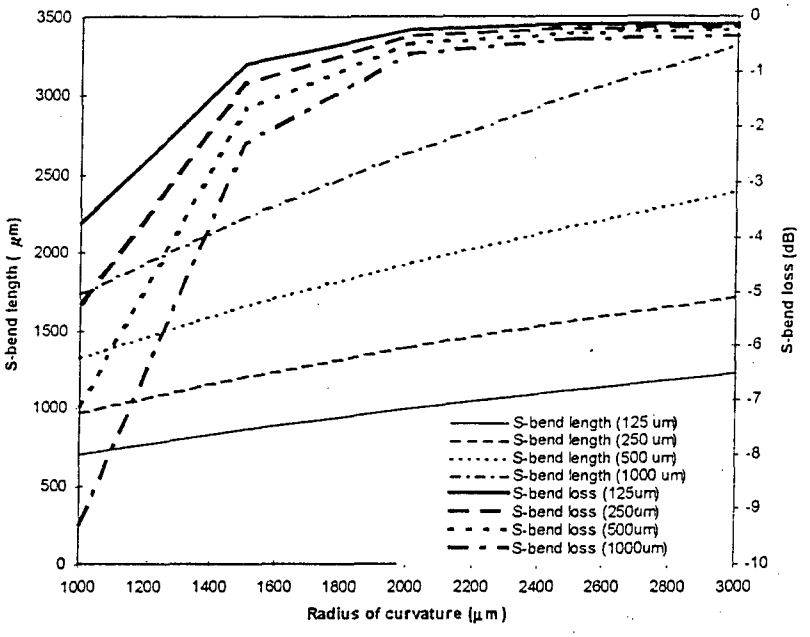

Figure 19. S-bend length and S-bend loss for different bend radii.

3.5 Summary of design parameters

In Table 4 below is a summary of the design parameters which will be used in Section 5 for analysis of the loss and signal-to-noise ratios for the 2x2 and 4x4 switch modules. We use a radius of curvature of R=2000 μm, which corresponds to a length of about 1000 μm for the 125 μm translation, and longer lengths for the larger translations. From Table 4, we can see that the splitter loss is about -3.1 dB for length greater than 1000μm. Channel crossings are small for crossing angles greater than 30°.

Channel property	Parameter	Loss
channel bends	R = 2000 μm	-0.16 dB/cm
splitter/combiner	splitter length >1000	-3.1 dB per splitter
channel crossing	crossing angle > 30°	< 0.1 dB loss per crossing

Table. 4. Summary of design parameters

4. Objective 3: Module design and alignment techniques

In this section, we analyze the coupling losses for the entire switch module for the two different configurations shown in Figure 20. In configuration 1, both the waveguides and SOAs are flip-chip bonded onto the substrate. In configuration 2, the waveguides are fabricated directly onto the substrate, and thus the waveguides can be photolithographically defined, and aligned, with respect to the V-grooves and the flip-chip bond pad metalization.

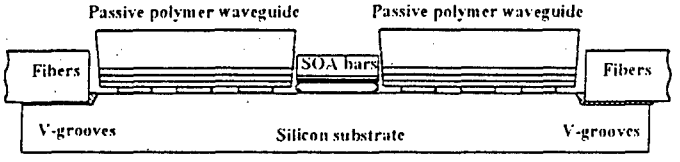

1) Configuration 1. Flip-Chip attachment of 3 elements.

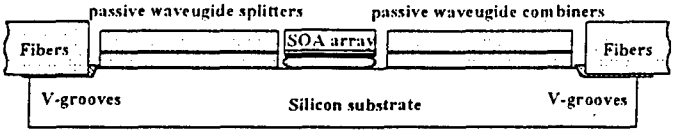

2) Configuration 2. Flip-Chip attachment of SOAs on substrate which contains the passive polymer waveguides.

Figure 20. Hybrid switch module integration techniques.

In order to determine the coupling efficiency of the entire switch module a Monte-Carlo analysis was used. We assume that the component placement has a misalignment with a Gaussian distribution. The Gaussian distribution is defined by

$$f(x) = \frac{1}{\sqrt{2\pi}\sigma} \exp\left(\frac{-x^2}{\sigma^2}\right). \tag{4.1}$$

We assume that the misalignment tolerance corresponds to the 2σ value of the Gaussian distribution. The 2σ tolerance value implies that there are 95.5% of the devices with a misalignment within the tolerance value.

For all of the misalignments, the offset between components is calculated by keeping track of the previous misalignment, since the misalignments are not independent of each other. Figure 21 shows how the misalignments are related, and how they are calculated for the x and y directions. As can be seen, there are 5 different components (2 fibers, 2 waveguides and 1 SOA) which need to be combined onto the substrate, all of which have misalignments associated with them. What is important is the offsets between the respective components. The offsets are calculated by taking the difference between the two adjacent components. The individual component misalignments are found from randomly generated numbers whose elements are normally distributed with mean 0 and 2σ value equal to the alignment tolerance. As can be seen in Figure 21, the individual misalignments are calculated with respect to the optical axis which corresponds to the line labeled $x=0$.

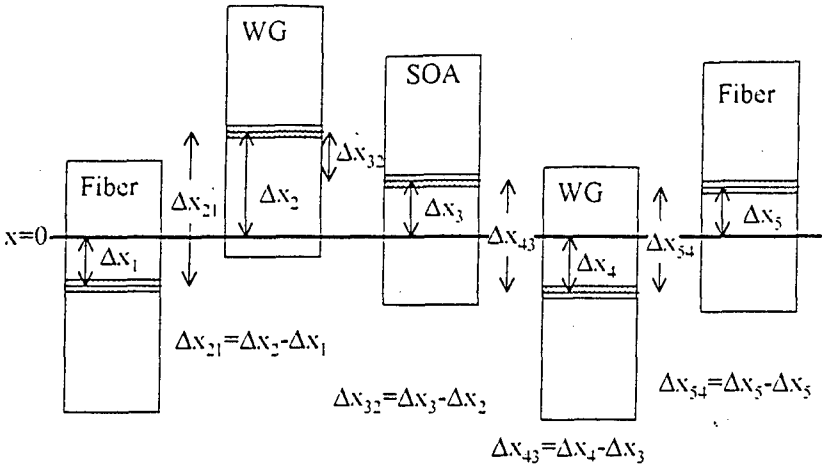

Figure 21. Misalignments of components in the hybrid switch for configuration 1.

In the z direction, the components separation is calculated in a similar way. In this case, the separation between the first and second components is

$$\Delta z_{21} = sep_{21} + \Delta z_2 - \Delta z_1 , \tag{4.2}$$

where sep_{21} is the nominal separation between the two components, and Δz_1 and Δz_2 are the misalignments of the respective components. The separations between the subsequent components are calculated in the same way.

The Monte Carlo analysis was run for 10,000 cases of randomly generated offsets for each individual component. The coupling efficiencies were then calculated between all of the individual components and were combined to get the overall coupling efficiency for the entire module. The coupling loss thus includes both the mode mismatch loss and the misalignment loss. In order to reduce computation time, the coupling efficiencies were first calculated between all of the components over a 3-dimensional grid.

The coupling efficiencies between all of the components were calculated for z separations between 0 and 10 μm with a sample spacing of 0.2 μm. The efficiencies were calculated in the x (lateral) direction from -6.5 to 6.5 μm with a sampling space of λ/8 (0.1625 μm), and y (vertical) direction from -3.25 to 3.25 μm, also with a sampling space of λ/8. Thus there were 160,000 coupling efficiencies that were calculated and stored in a 3-dimensional array for each of the component pairs (fiber-to-waveguide, waveguide-to-SOA, SOA-to-waveguide, and waveguide-to-fiber). The coupling efficiencies for a given misalignment was then found by accessing the corresponding element of the array. This was done so that the coupling efficiencies had to be calculated only once instead of calculating the individual coupling efficiencies for each misalignments during the Monte Carlo analysis which would require much more computation time, since the field would have to be propagated between each component. Since the Rayleigh-Sommerfeld propagation is the most computationally expensive step, the field was be propagated to one plane, and then all of the coupling efficiencies for that plane could be calculated.

The Gaussian fiber approximated profile was used for the fiber, and the optimized 6x6 μm channel distribution was used for coupling between the fiber and waveguide. The optimized 3x3 μm channel field was used to calculated the coupling between the waveguide and SOA. Both the 6x6 and 3x3 optimized channels were found in Section 2.

4.1. Monte Carlo results for configuration 1

The following misalignment tolerances were used for all of the components in the Monte Carlo analysis for the coupling calculations for configuration 1:

x tolerance ($2\sigma_x$)=2 μm
y tolerance ($2\sigma_y$)=1 μm
z tolerance ($2\sigma_z$)=2 μm
waveguide to fiber nominal separation=5 μm
waveguide to SOA nominal separation=5 μm

The coupling losses were calculated for the entire module, keeping track of the losses before and after the SOA. Figure 22 shows the coupling losses both before and after the SOA. We would expect the pre-SOA and post-SOA losses to be similar since we are coupling between the same structures, but as can be seen from Figure 22, the post SOA loss is slightly lower that the pre SOA loss. The reason for the slight coupling difference is because the SOA-to-waveguide coupling losses are larger than the waveguide-to-SOA loss, since the waveguide mode expands slower than the SOA mode (the waveguide mode is larger than the SOA mode). The minimum pre SOA loss was found to be -3.09 dB, and the minimum post SOA loss was -2.95 dB. Table 5 shows the same results for selected yield values.

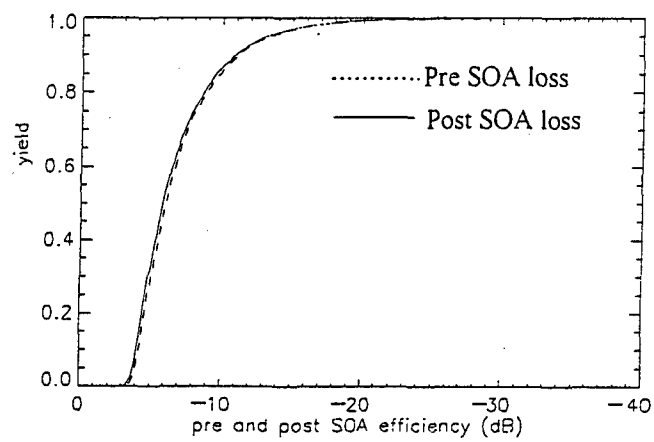

Figure 22. Yields vs. loss both before and after the SOA in the module.

In Figure 23, we can see the yield vs. total module loss of the entire module. The minimum total module loss was found to be -6.78 dB, so the yield is 0% for losses less than -6.78dB. We can see that there is a yield of about 20% for a module loss of -10dB. Table 5 includes entire module losses for selected yield values.

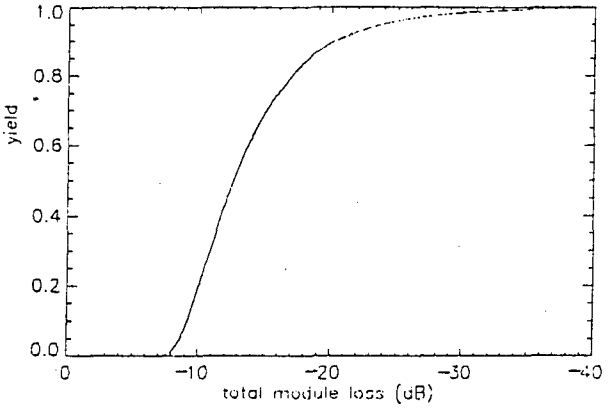

Figure 23. Yields vs. loss for the entire module.

Yield	Pre SOA loss (dB)	Post SOA loss (dB)	Total loss (dB)
0.1	-4.28291	-4.07823	-9.20819
0.2	-4.698	-4.49772	-10.0436
0.3	-5.10042	-4.90797	-10.8619
0.4	-5.54396	-5.36107	-11.6749
0.5	-6.03801	-5.9176	-12.5964
0.6	-6.67562	-6.59556	-13.6653
0.7	-7.54487	-7.47147	-15.0864
0.8	-8.82729	-8.79426	-16.9897
0.9	-11.0791	-10.8619	-20.4576

Table 5. Losses for different yield values for configuration 1.

4.2. Monte Carlo results for configuration 2

In this section, we run the Monte Carlo analysis for the second configuration which has the waveguides made directly on the substrate. By looking at Figure 24, we can see that the offsets in the x and y directions are the same as in configuration 1, but with the misalignments of the waveguide sections set to zero. Thus Δx_2, Δy_2, Δx_4, Δy_4 are all assumed to be zero since the waveguides are photolithographically defined directly on the substrate. There is a slight difference in the component separations compared to configuration 1. There is now a different relationship among the separations between the first waveguide section and the SOAs, and between the SOA and second waveguide section. The sum of those two separations is constant (the SOA is placed in a gap between the two waveguide sections). We assume a total gap between SOA and waveguide sections of 10 μm (sum of the waveguide to SOA separation and SOA to waveguide separation). We use the same values for the x, y, and z tolerances ($2\sigma_x$=2, $2\sigma_y$=1, $2\sigma_z$=2) as for configuration 1, and again assume a waveguide to fiber nominal separation of 5 μm.

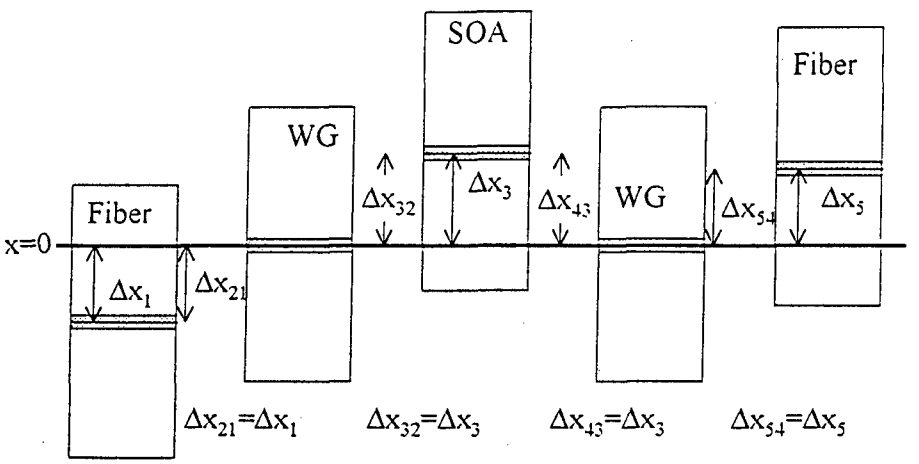

Figure 24. Misalignments for configuration 2.

The Monte Carlo analysis was again run for 10,000 cases of randomly generated offsets for each individual component. The results can be seen in Figure 25, with selected values shown in Table 6. As can be seen by comparing with the results from coupling losses for configuration 1, the losses are lower for configuration 2. For example in configuration 2, the yield is about 60% for a module loss of -10dB, compared to the 20% yield seen for configuration 1. The coupling losses are lower since the waveguide sections are fabricated directly on the substrate, and thus the misalignments lessened. The minimum pre-SOA, post-SOA and total loss were found to be the same as for configuration 1. This is expected, since these values correspond to a case where all of the components have minimal misalignments. The difference is that the 'best case' occurs more frequently in configuration 2, which manifests itself in the higher yield. Since the coupling losses are lower for configuration 2, we conclude that configuration 2 is the more desirable of the two configurations, although the fabrication is perhaps more difficult. Configuration 2 requires etching of the waveguide channels to make the gap for the placement of the SOA array.

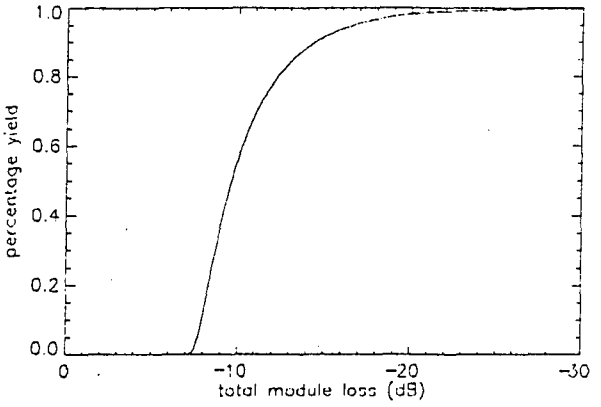

Figure 25. Yield vs. module loss for configuration 2.

Yield	Pre SOA loss (dB)	Post SOA loss (dB)	Total loss (dB)
0.1	-3.99027	-3.80907	-7.9588
0.2	-4.23659	-4.03403	-8.35647
0.3	-4.44906	-4.25969	-8.72895
0.4	-4.698	-4.47332	-9.17215
0.5	-4.93495	-4.74955	-9.70616
0.6	-5.27244	-5.0724	-10.3152
0.7	-5.70248	-5.49751	-11.1351
0.8	-6.28932	-6.07303	-12.3657
0.9	-7.30487	-7.12198	-14.5593

Table 6. Losses for configuration 2.

5. Objective 4: Array size in view of device SNR

In order to determine a reasonable individual switch module array size, there are several things that must be considered. We must first find the entire loss through the module. The entire module loss is calculated using the results from Section 3 and Section 4, in which the waveguide losses and the coupling losses due to misalignments were found. We can then find the maximum number of 2x2 and 4x4 switch module stages that can be cascaded. The maximum number of 2x2 stages allows us to find the size of a switch network that can be built using the 2x2 switch module as a building block to make a larger network.

5.1. Larger switch network using 2x2 switch module as building block

We can make a larger switching network using a smaller switch module as a building block. An example of such a large network is shown in Figure 26. This network is called the Benes network and is made up of 2x2 switch modules. The Benes network is rearrangeably non-blocking and uses $2\log_2 N-1$ stages, with N/2 switches per stage, for an NxN switch [68]. For example, a 128x128 Benes network needs 13 stages and a 4096x4096 needs 23 stages.

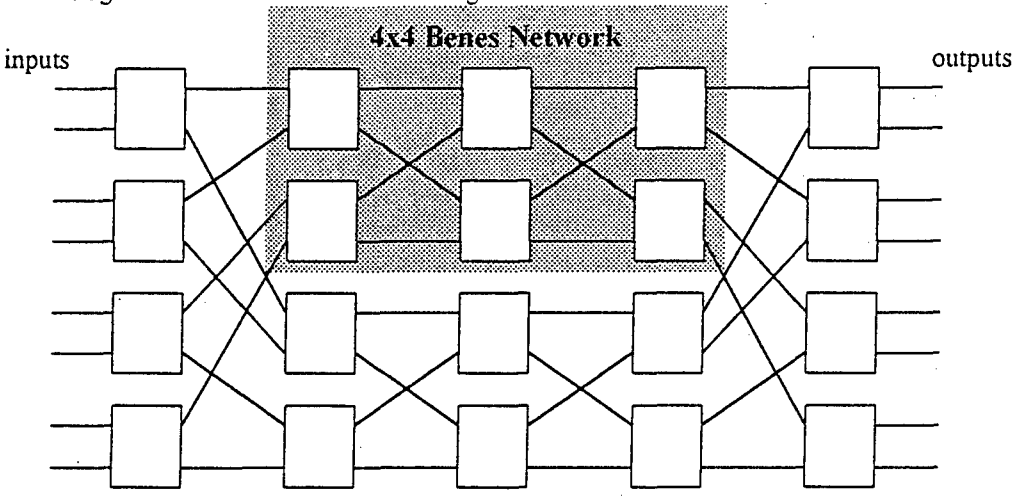

Figure 26. Benes network.

5.2. Total module loss

In order to determine the entire module loss, we use the results from Sections 3 and 4. The loss due to channel crossing is a function of the crossing angle. The crossing angle of 2 S-bends as a function of the offset between the two S-bends, with the same radius of curvature, is given by:

$$\theta = 2\cos^{-1}\left(\frac{R-\frac{offset}{2}}{R}\right) \tag{5.1}$$

where *offset* is the separation between the two crossing S-bends. Once the angle between the channels is known, then the loss due to the channel crossing were found by using the data from Section 3.3, in which the loss due to channel crossings was found. The loss for different angles were interpolated from the data in Figure 16.

To calculate the losses in the waveguide due to splitters, combiners, channel loss and channel bends, we use the data from Section 3.2 and 3.4. The distance between SOAs in the SOA array were assumed to be 250 μm. When finding the loss associated with the modules, we calculated the loss using a radius of

curvature of 2000 μm, since this radius has been shown to produce a lower loss while keeping the module as short as possible.

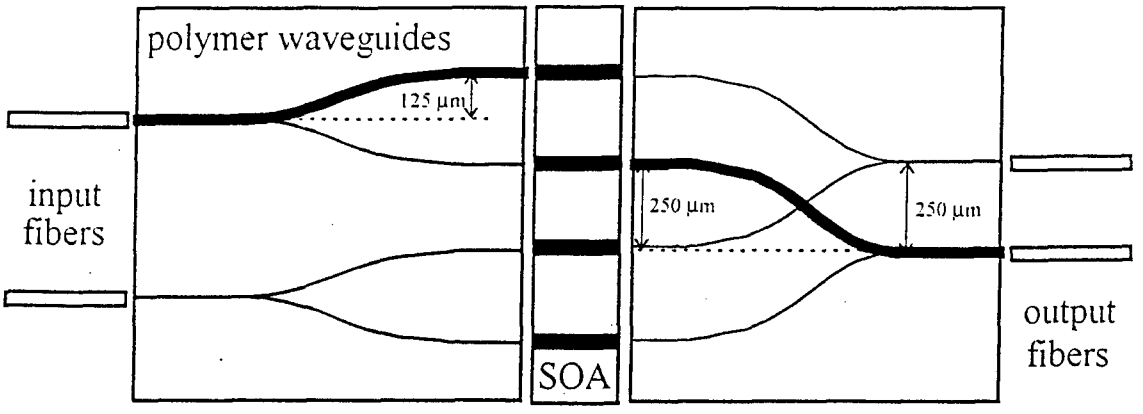

Figure 27. 2x2 switch module showing channel separations and worst case channel pathway.

Figure 27 shows the S-bend translation distance for the 2x2 switch module, as well as the separation between the crossing S-bend channels. The S-bend loss from Figure 19 was used (R=2000μm) for the S-bend translation of 125 μm at the input waveguide section, and for the S-bend translation of 250 μm for the output waveguide section. The crossing in the output waveguide section was calculated using equation (5.1) for an offset of 250 μm, with interpolated data from Figure 16 used to calculate the associated loss. The length of the S-bend from Figure 19 was used to calculate the channel loss using a value of -0.1dB/cm (loss due to material absorption, sidewall scattering and other imperfections). For each splitter and combiner, we added an additional loss of 0.1 dB, as calculated in Section I, to the ideal -3dB loss, yielding a splitter and combiner a loss of -3.1 dB. For the 2x2 module, the losses in the waveguide section are summarized as in Table 7, using the worst case channels which are shown in bold in Figure 27.

	Loss mechanism	Loss (dB)
pre SOA loss	S-bend loss (125 μm translation)	-0.155
	Splitter loss	-3.1
	Channel crossing	0
	Channel loss	-0.0992
	Total pre SOA loss	**-3.3542**
post SOA loss	S-bend loss (250 μm translation)	-0.2175
	Combiner loss	-3.1
	Channel crossing (40.7° angle)	-0.057054
	Channel loss	-0.1392
	Total pre SOA loss	**-3.54406**

Table 7. Summary of 2x2 waveguide losses.

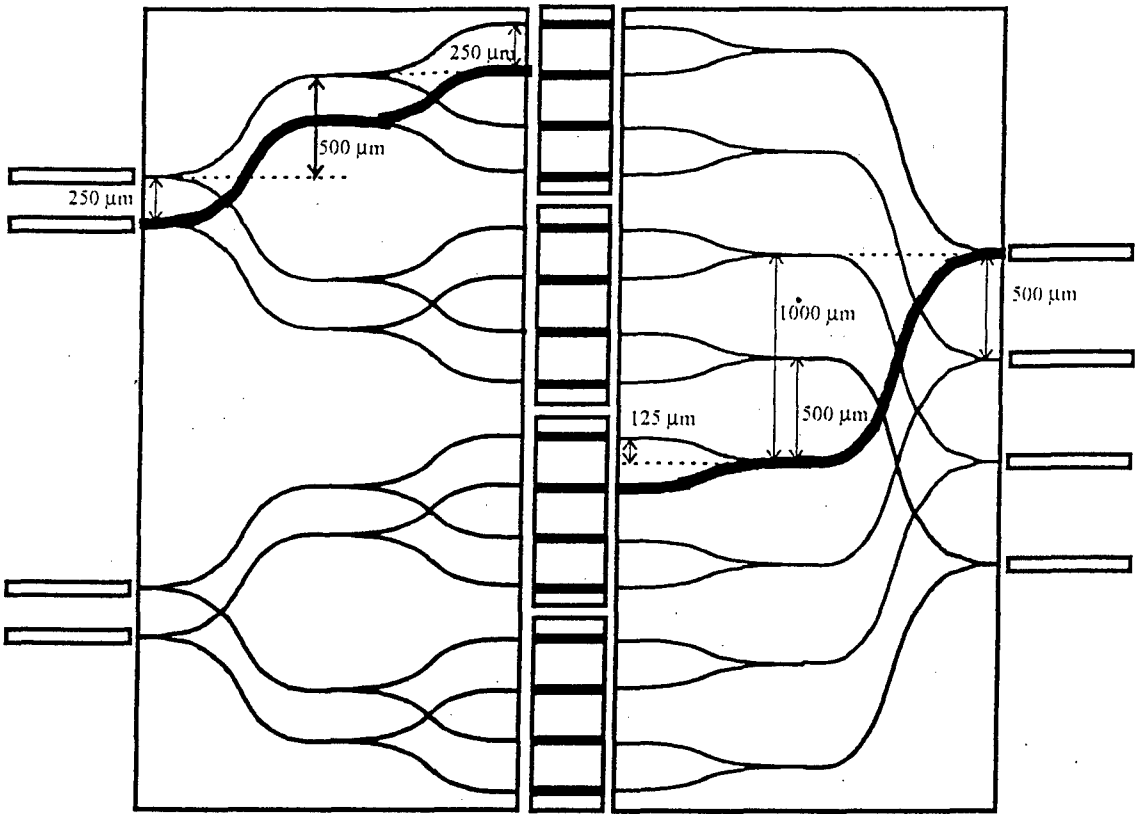

Figure 28. 4x4 switch module showing channel separations and worst case channel pathway.

The same loss analysis can be performed for the 4x4 switch module for the worst case channel shown in bold in Figure 28. We can see that the worst case pre-SOA channel has 2 channel crossings, and the worst case post-SOA channel contains 3 channel crossings, at 2 different angles. The total loss for the 4x4 module is summarized in Table 8.

	Loss mechanism	Loss (dB)
pre SOA loss	S-bend loss (500 µm translation)	-0.3025
	Splitter loss	-3.1
	Channel crossing 1 (40.7° angle)	-0.057054
	S-bend loss (250 µm translation)	-0.2175
	Splitter loss	-3.1
	Channel crossing 2 (40.7° angle)	-0.057054
	Channel loss	-0.3328
	Total pre SOA loss	**-7.167**
post SOA loss	S-bend loss (125 µm translation)	-0.155
	Combiner loss	-3.1
	Channel crossing 1 (57.9° angle)	-0.040606
	Channel crossing 2 (82.8° angle)	-0.033185
	Channel crossing 3 (57.9° angle)	-0.040606
	S-bend loss (1000 µm translation)	-0.41344
	Combiner loss	-3.1
	Channel loss	-0.3638
	Total pre SOA loss	**-7.247**

Table 8. Summary of 4x4 waveguide losses.

We can now combine the waveguide loss together with the coupling losses between the different components (Monte Carlo analysis) to get the total module loss which includes channel loss, bend loss, channel crossing, splitter loss, and combiner loss and coupling losses. In Figure 29 we can see the total module loss as a function of the yield for the 2 module attachment configurations. For both configurations, the total loss increases as the yield increases. By observing the losses for the 2 configurations, we see that configuration 2 produces lower overall loss in the module, due to better coupling characteristics. There is about a 2 dB difference in the module loss for a 20% yield, increasing to about a 4 dB difference in loss for the 80% yields.

If we assume a maximum SOA gain of 28 dB, we can see that the gain can overcome the losses for all of the 2x2 module yields, and most of the 4x4 switch module yields. For an 8x8 switch, however, there would be an additional loss of at least 6.2 dB due to an additional splitter and combiner, making the loss difficult to overcome. We therefore center our attention on a maximum switch module size of 4x4.

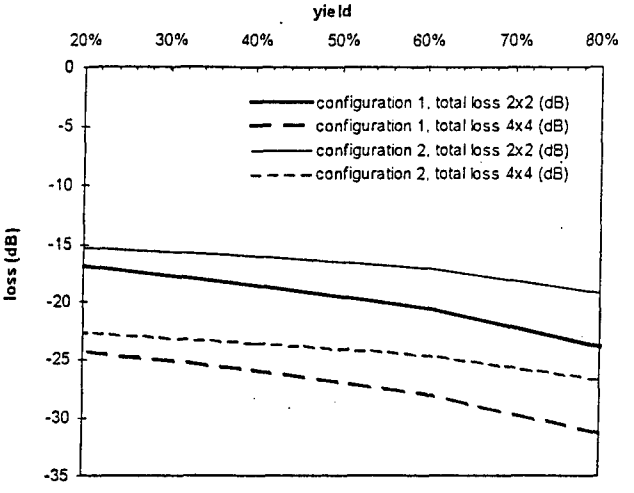

Figure 29. Total module loss including waveguide losses and coupling losses.

5.3. Noise and bit error rate (BER)

There are several noise contributors in the switch including channel crosstalk, signal extinction ratio, and amplifier noise. However, the amplifier noise, or amplified stimulated emission (ASE), dominates over the other noise mechanisms in most SOA switch systems. The ASE power is given by

$$P_{sp} = p \cdot S_{sp} \cdot \Delta v_{sp}, \tag{5.2}$$

where Δv_{sp} is the effective band width of the spontaneous emission and p is the number of modes which is 2 for a polarization insensitive amplifier (TE and TM). S_{sp} is the spectral density of the spontaneous emission given by

$$S_{sp} = n_{sp}(G-1)hv. \tag{5.3}$$

And n_{sp} is the amplifier population-inversion parameter. A complete list of the parameters can be seen in Table 9.

The ASE manifests itself in the form of beating terms with the signal, with itself and with the shot noise in the detector. These three noise terms are the signal-spontaneous beating [69]

$$\sigma^2_{sig-sp} = 4R^2 G P_s S_{sp} \Delta f, \tag{5.4}$$

the spontaneous-spontaneous beating

$$\sigma^2_{sp-sp} = 4R^2 S^2_{sp} \Delta v_{opt} \Delta f, \tag{5.5}$$

and the shot-spontaneous beating

$$\sigma_{s-sp}^2 = 4qRS_{sp}\Delta f \,. \tag{5.6}$$

There is also the shot noise

$$\sigma_s{}^2 = 2q(R(GP_s + P_{sp}) + I_d)\Delta f \,, \tag{5.7}$$

and the thermal noise in the detector

$$\sigma_T{}^2 = \frac{4k_B T}{R_L}\Delta f \,. \tag{5.8}$$

The total noise current contribution is

$$\sigma_{total}{}^2 = \sigma_{sig-sp}{}^2 + \sigma_{sp-sp}{}^2 + \sigma_{s-sp}{}^2 + \sigma_s{}^2 + \sigma_T{}^2 \,. \tag{5.9}$$

In order to design a system, there needs to be a design criteria. One such criteria that can be used the BER which is determined by [70]

$$BER = \frac{1}{2}\,\mathrm{erfc}\left(\frac{Q}{\sqrt{2}}\right). \tag{5.10}$$

where erfc is the complementary error function and

$$Q = \frac{I_1 - I_0}{\sigma_1 + \sigma_0} \,. \tag{5.11}$$

Parameter List	
Δf	Electrical bandwidth
$\Delta \nu_{sp}$	Spontaneous emission bandwidth
$\Delta \nu_{opt}$	Optical filter bandwidth
R	Receiver responsivity ($\eta q/h\nu$)
η	Quantum efficiency of detector
q	Electron charge
$h\nu$	Photon energy
p	Number of modes
G	Amplifier gain
S_{sp}	Spontaneous emission spectral density
P_{sp}	Spontaneous emission power
P_s	Signal power
n_{sp}	Population-inversion parameter
I_d	Detector dark current
k_B	Boltzmann constant
T	Temperature (K)
R_L	Load resistor
I_1	Signal current for a "1" bit
I_0	Signal current for a "0" bit
σ_1	Noise current for a "1" bit
σ_0	Noise current for a "0" bit

Table 9. Parameter list

5.4. Maximum number of stages using switch module

In order to determine the maximum number of switches which can be cascaded in order to form a larger switching network, we calculated the BER through multiple stages of the hybrid switches using the model described in Section 5.3. Figure 30 illustrates a cascaded switch system of N cascaded stages. For the ASE calculation and propagation, the spontaneous emission bandwidth ($\Delta\nu_{sp}$) is used to calculate the spontaneous emission power which propagates through the system of N stages until it reaches the optical filter ($\Delta\nu_{opt}$) placed before the detector. The thermal noise in the detector is calculated with a temperature of 300 °K. In calculating the maximum number of cascadable stages of 2x2 and 4x4 stages, we require that the BER remain below a value of 10^{-9}. An optical filter bandwidth of 1 nm was used. The analysis was performed with the amplifier saturating according to

$$G = G_o\left(-\frac{G-1}{G}\frac{P_{out}}{P_s}\right) \tag{5.12}$$

where G is the gain, G_o is the unsaturated gain, P_{out} is the output power and P_s is the saturation power.

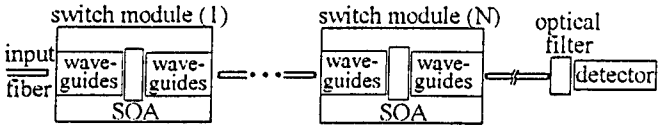

Figure 30. N cascaded stages of optical switch modules.

The SOAs are assumed to be polarization insensitive optical amplifiers operating at a wavelength of 1.3 μm. There are several such amplifiers being developed and some being sold commercially. The other amplifier parameters that were used are n_{sp}=3, a maximum gain of value of 28 dB, and a saturation output power of +10 dBm. The signal coming into the switch was assumed to have an infinite extinction ratio so that the effects of the propagating ASE would be more evident.

As we have seen, there are many sources of loss and only one source of gain, the SOA. A switch (or other device) that has no net loss is also referred to as transparent. The reflections were seen to affect the operation of an optical SOA switch [13], and must be significantly reduced in order to have a good, working switch. For this switch system model, the reflection losses were neglected. The total loss from all of the loss mechanisms were combined into two loss parameters per switch module. The first loss parameter includes the losses in the switch module before the SOA, and the second parameter includes the losses after the SOA. This was done since the amplified spontaneous emission (ASE) noise is only affected by the loss after the SOA in the module. The signal power, however, is degraded by the pre-SOA loss as well as the post-SOA loss.

5.4.1. Maximum number of cascadable 2x2 switch modules

We first analyze the 2x2 switch module, to find the maximum number of cascadable stages. In order to find the maximum number of stages, we performed simulations of the entire module using the losses from the Section 5.2. There are two different mechanisms that limit the number of stages that can be cascaded. The first the bit error rate (BER) and the second is the amplifier saturation. In order to see some of the salient features of how many stages can be cascaded, we begin by showing the maximum number of stages of cascaded 2x2 switches for a 40% device yield for configuration 1. As can be seen from Table 5 above, there is -11.68 dB loss due to misalignment for a 40% yield using configuration 1. We can also see that there is -0.2542 dB loss in the waveguide section before the SOA and -0.444 dB loss in the waveguide section after the SOA. It is important to know that amount of loss that occurs before and after the SOA, since this will effect the SOA saturation and gain characteristics. If we assume that the coupling loss from misalignments is evenly distributed before and after the SOA, then there will be -6.0942 dB loss before the SOA and -6.284 dB loss after the SOA.

In Figure 31, the maximum number of stages is plotted against the input power to the first module for several different gains (losses) through the entire switch. The simulations were run with a BER requirement of 10^{-9}, a bit rate of 10 GHz, and an optical filter bandwidth of 1nm placed before the detector. The curve for -0.0 dB loss corresponds to a transparent switch, where the gain in the SOA compensates for all of the losses due to the misalignments and waveguide losses. It can be seen that the maximum number of stages occurs for the case where there is actually -0.05 dB loss through the switch module. The maximum number of stages increases with increasing input power up to a certain point. For this portion of the curve, the maximum number of stages is limited by the bit error rate requirement. Once the input power reaches a certain point, the maximum number of stages begins to decrease. At this point, the maximum number of stages begins to be limited by the amplifier saturation. For the case of the transparent switch, it can be seen that the amplifier saturation begins to take effect for an input power of about -3 dBm. For the case of 0.05 dB loss per amplifier stage, the saturation effects begin for an input power of 5 dBm. The SOA saturation is more predominant for the case of the transparent switch because the ASE power which is added at each stage continues to grow, whereas the signal power remains constant (the gain at each stage is defined as the gain of the signal). So for the transparent switch, the signal power remains constant, but the ASE grows, thus increasing the total power input to each switch, and the amplifiers begin to saturate sooner. When there is a little bit of loss in each switch module, the signal power decreases slightly, and the ASE still grows, but in this case the total input power (sum of the signal power and ASE power) is lower, and thus the amplifiers saturate for a larger input power.

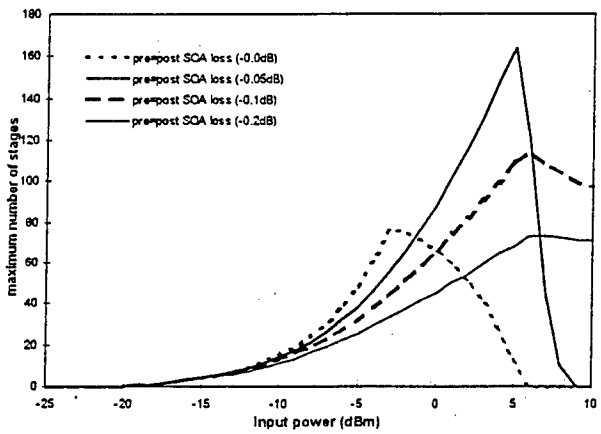

Figure 31. Maximum number of 2x2 switch stages for a 40 % device yield (configuration 1) for several different overall module gains.

For the previous graph in Figure 31, we saw the maximum number of stages, under the assumption that the loss due to coupling was equally distributed before and after the SOA. However, this will not be the case in reality. There are two extreme cases to look at as well, using the entire coupling losses calculated from the Monte Carlo analysis for the entire module. The first case is that with the minimum loss of -3.09 dB before the SOA (best coupling efficiency before the SOA), with the remainder of the loss after the SOA. The second case is that of having the minimum loss of -2.95 dB after the SOA with the remainder at the input. The 3 different cases are summarized in the Table 10 below. As can be seen, the total module loss corresponding to the 40% yield case are the same, with the difference being how the coupling loss is distributed before and after the SOA.

	Pre SOA coupling loss (dB)	Post SOA coupling loss (dB)	Pre SOA channel loss (dB)	Post SOA channel loss (dB)	Total module loss (dB)
minimum pre SOA loss	-3.09	-8.59	-0.2542	-0.444	-12.38
post SOA loss	-5.84	-5.84	-0.2542	-0.444	-12.38

= pre SOA loss					
minimum post SOA loss	-8.73	-2.95	-0.2542	-0.444	-12.38

Table 10. Distribution of loss before and after the SOA (configuration 1).

Simulations were run assuming these three different cases, again using a BER requirement of 10^{-9}, a bit rate of 10 GHz, and an optical filter bandwidth of 1nm placed before the detector. Figure 32 shows the results of the three different cases with a module loss of -0.05 dB. The case of the pre SOA and post SOA losses being equal is the same as that seen in Figure 31 for the module loss of -0.05 dB. We can also see that the case of the minimum pre SOA loss has a maximum number of stages which occurs for the lowest input power. And the case with the minimum post SOA loss has a maximum number of stages that occurs for the highest input power. The case with the pre SOA and post SOA loss being equal has its peak that occurs between the two extreme cases. In order to be sure that the number of stages is valid for all of the switches with the 40% yield, we use the two extreme cases as the bounds for the number of stages. We essentially look at the overlap between the two curves for the extreme cases. This is shown in the graph, labeled as 'bounds', and corresponds to the overall maximum number of stages for the switch module with a 40% yield in configuration 1.

If we have a requirement of using a range of input powers, then the maximum number of stages can also be found. By looking at Figure 32, for a maximum of 40 cascadable stages, there is an input range of about -2 dBm to 4 dBm. This range is shown as the shaded area in the graph.

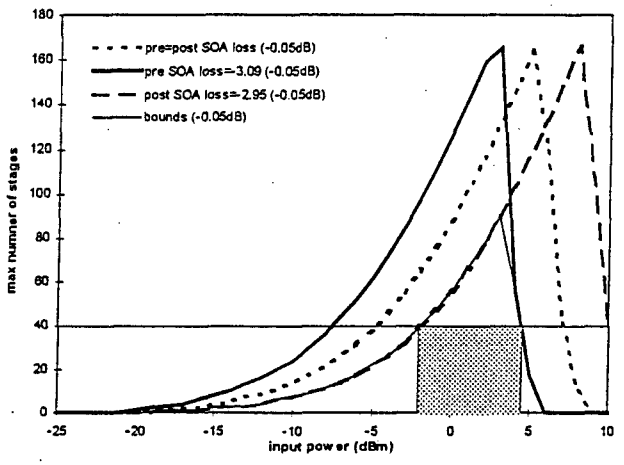

Figure 32. Maximum number of stages for 40% yield using configuration 1.

In Figure 33, we can see the maximum number of stages for different module losses, taken from the bounds of the two extreme cases as was done in Figure 32. We can see that there is the same kind of characteristics as was seen in Figure 31. The maximum number of stages is limited by the BER for low input powers and then becomes limited by the SOA saturation as the input power increases. It can be seen that in order to choose which overall module gain is the best depends upon the input power. For example, if the input power to the first stage is -2 dBm, then the transparent switch is the best choice, however if the input power to the first switch is 5 dBm, then the switches with a -0.1 dB loss per module becomes the obvious choice.

PAGE 34, 36, 37

IS

MISSING

IN

ORIGINAL

DOCUMENT

5.4.2. Maximum number of cascadable 4x4 switch modules

In Figure 35 we can see the maximum number of 4x4 cascadable switch modules for different device yields. The maximum number of stages is again shown for an input power of 0 dBm to the first stage. For the case of the 20% yield, configuration 1, there is a maximum of 15 stages, and for the 80% yield, there is a maximum of only 2 stages at 0 dBm. Again configuration 2 yields a higher maximum number of stages compared with the same yield for configuration 1. Since the 4x4 switch module losses in the waveguide section are much higher that in the case of the 2x2 switch, the number of stages is greatly decreased.

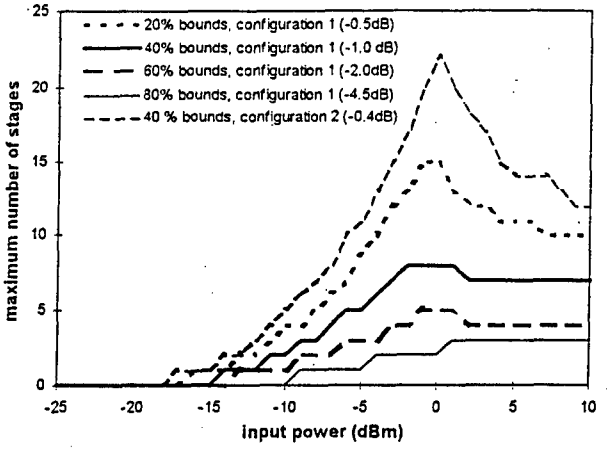

Figure 35. Maximum number of cascadable 4x4 switch modules for different module yields.

5.4.3. Effect of filter bandwidth and bit rate on the maximum number of stages

The filter bandwidth and the bit rate both effect the maximum number of stages which can be cascaded, since they both effect the BER of the system. As can be seen in Figure 36, which shows the maximum number of stages for different filter bandwidths, the maximum number of stages increases as the filter bandwidth decreases. The BER decreases as the filter bandwidth decreases since the filter has the effect of limiting the amount of ASE power which makes it to the detector. A smaller optical filter bandwidth filters out more of the ASE. The saturation of the SOAs is not affected, as can be seen from the same bound on the gain saturation limiting side of the curves.

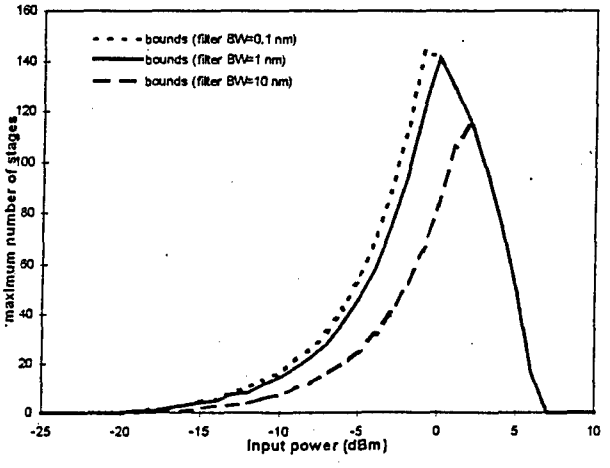

Figure 36. Effect of the optical filter bandwidth on the maximum number of stages.

PAGE 34, 36, 37

IS

MISSING

IN

ORIGINAL

DOCUMENT

There is also an issue with polymer waveguide materials. We have had the opportunity to use PMMA/DR1 as well as Amoco Ultradel 4212 with DCM dye., and Ultradel 9020D. We have, however, had several processing difficulties associated with making the 3-domensional taper structure. In addition to these polymers, there are also other polymer materials which are currently being investigated including acrylates, polyimides, siloxane polymers, as well as several other polymer material systems.

12. Future work

There is still work which can be done with respect to building the hybrid integrated SOA optical switch. It would be important to evaluate new polymer materials to find a material that has good optical qualities and processing properties which are compatible with the module fabrication. It is imperative to acquire and characterize SOA devices. It would also be useful to make a prototype hybrid switch module which would help reveal other potential issues involved with the switch operation and fabrication.

13. References

[1] M. Ikeda, "Laser Diode Switch," *Electronics Letters*, vol. 17, no. 23, pp. 899-900, 1981.

[2] A. Himeno and M. Kobayashi, "4x4 Optical-Gate Matrix Switch," *Journal of Lightwave Technology*, vol. LT-3, no. 2, pp. 230-235 1985.

[3] W. Hunziker, "Packaging of Optoelectronic Components," Proc. 2nd Workshop on Electronics for LHC Experiments, Balatonfured, Hungary, September 1996, pp. 365-372

[4] M.G. Young, U. Koren, B.I. Miller, M. Chien, M.A. Newkirk, J.M. Verdiell, "A compact 2x2 amplifier switch with integrated DBR lasers operating at 1.55 μm," *IEEE Photonics Technology Letters*, vol.4, no.9, p. 1046-8, 1992.

[5] F. Dorgeuille, B. Mersali, M. Feuillade, S. Sainson, S. Slempkès, M. Foucher, M., "Novel approach for simple fabrication of high-performance InP-switch matrix based on laser-amplifier gates," *IEEE Photonics Technology Letters*, vol.8, no.9, p. 1178-80, 1996.

[6] J.D Burton, P.J. Fiddyment, M.J. Robertson, P. Sully, "Monolithic InGaAsP-InP laser amplifier gate switch matrix," *IEEE Journal of Quantum Electronics*, vol.29, no.6, p. 2023-7, 1993.

[7] M. Janson, L. Lundgren, A.-C. Morner, M. Rask, M.; B. Stoltz, M. Gustavsson, L. Thylen, "Monolithically integrated 2x2 InGaAsP/InP laser amplifier gate switch arrays," *Electronics Letters*, vol.28, no.8, p. 776-8, 1992.

[8] C. Holtmann, T. Brenner, R. Dall'Ara, P.A. Besse, H. Melchior, "Monolithically integrated semiconductor optical amplifiers for transparent 2x2 switches at 1.3 micrometer," *Mitteilungen AGEN*, no.56-57, p. 45-8, 1993.

[9] K. Hamamoto, K. Komatsu, "Insertion-loss-free 2x2 InGaAsP/InP optical switch fabricated using bandgap energy controlled selective MOVPE," *Electronics Letters*, vol.31, no.20, p. 1779-81.

[10] Kwan Ryong Oh, Joo-Heon Ahn, Jeong Soo Kim, Seung Won Lee, Hong Man Kim, Kwang Eui Pyun, Hyang Moo Park "2x2 InGaAsP/InP laser amplifier gate switch arrays using reactive ion etching," *Electronics Letters*, vol.32, no.1, p. 39-40.

[11] W. van Berlo, M. Janson, L. Lundgren, A.-C. Morner, J. Terlecki, M. Gustavsson, P. Granestrand, P. Svensson, P., "Polarization-insensitive, monolithic 4x4 InGaAsP-InP laser amplifier gate switch matrix," *IEEE Photonics Technology Letters*, vol.7, no.11, p. 1291-3, 1996.

[12] E. Almstrom, C. P. Larsen, L. Gillner, W. M. Van Berlo, M. Gustavsson, E. Berglind, "Experimental and analytical evaluation of packaged 4x4 InGaAsP/InP semiconductor optical amplifier gate switch matrices for optical networks," *Journal of Lightwave Technology*, vol.14, no.6, p. 996-1004, 1996.

[13] Y. Yamada, H. Terui, Y. Ohmori, M. Yamada, A. Himeno and M. Kobayashi, "Hybrid-Integrated 4x4 Optical Gate Matrix Switch Using Silica-Based Waveguides and LD Array Chips," *Journal of Lightwave Technology*, vol. 10, no. 3, pp. 383-389, 1992.

[14] R. F. Kalman, L. G. Kazovsky and J. W. Goodman, "Space Division Switches Based on Semiconductor Optical Amplifiers", *IEEE Photonics Technology Letters*, vol. 4, no. 9, pp. 1048-1051, 1992.

[15] N.A. Olsson, "Lightwave Systems with Optical Amplifiers," *Journal of Lightwave Technology*, vol. 7, no. 7, pp. 1071-1082, 1989.

[16] M. Ikeda, "Maximum Number of Connectable Laser Diode Optical Switch (LDSW) Systems," *Optical and Quantum Electronics*, vol. 20, pp. 515-524, 1988.

[17] Lars Gillner and Lars Thylén, "Effect of Gain saturation in Semiconductor Laser Amplifier Links," *IEEE Photonics Technology Letters*, vol. 4, no. 5, pp. 438-441, 1992.

[18] G. Jeong and J. W. Goodman, "Gain Optimization in Switches Based on Semiconductor optical Amplifiers," *Journal of Lightwave Technology*, vol. 13, no. 4, pp. 598-605, 1995.

1. AGENCY USE ONLY (Leave blank)	2. REPORT DATE	3. REPORT TYPE AND DATES COVERED
	23 Dec. 98	Final

4. TITLE AND SUBTITLE
Integrated Optoelectronic Switching Technology for Fiber-Optic Communications Networks

5. FUNDING NUMBERS
DASG60-97-M-0209

6. AUTHOR(S)
Regis Fan and R. Brian Hooker

7. PERFORMING ORGANIZATION NAME(S) AND ADDRESS(ES)
University of Colorado
Astarte Fiber Networks, Inc.
Boulder, Colorado

8. PERFORMING ORGANIZATION REPORT NUMBER
N/A

9. SPONSORING/MONITORING AGENCY NAME(S) AND ADDRESS(ES)
U.S. Army Space and Missile Defense Command
P.O. Box 1500
Huntsville, Alabama 35807

10. SPONSORING/MONITORING AGENCY REPORT NUMBER
N/A

11. SUPPLEMENTARY NOTES
NONE

12a. DISTRIBUTION/AVAILABILITY STATEMENT
NONE

DISTRIBUTION STATEMENT A
Approved for Public Release
Distribution Unlimited

12b. DISTRIBUTION CODE
NONE

13. ABSTRACT (Maximum 200 words)

Optical switching can be performed by using optical amplifiers combined with a passive waveguiding network. Recently, most of the effort in optical amplifier switch modules have been focused on monolithic switches in which the entire device is fabricated on an InP substrate together with the semiconductor optical amplifiers (SOAs). In this paper, we investigate the use of SOAs with passive polymer waveguides to make hybrid switches of varying sizes. The optical amplifiers serve a dual purpose. The SOAs are used in order to gate the signal and amplify the signal in order to offset the losses associated with the passive waveguide elements as well as the losses from component misalignments in the switch module. Our analysis finds the largest switch module size that can be made with the architecture used. We also calculate the maximum number of switch modules which can be cascaded in order to retain a bit error rate (BER) under 10^{-9}.

14. SUBJECT TERMS	15. NUMBER OF PAGES
Polymer waveguides; optoelectronic switching; fiber-optic networks	38
	16. PRICE CODE

17. SECURITY CLASSIFICTION OF REPORT	18. SECURITY CLASSIFICATION OF THIS PAGE	19. SECURITY CLASSIFICATION OF ABSTRACT	20. LIMITATION OF ABSTRACT
unclassified	unclassifed	unclassified	SAR